

# ITERATIVE METHODS OF LINEARIZED MOMENT EQUATIONS FOR RAREFIED GASES \*

XIAOYU DONG<sup>†</sup> AND ZHENNING CAI<sup>‡</sup>

**Abstract.** We study the iterative methods for large moment systems derived from the linearized Boltzmann equation. By Fourier analysis, it is shown that the direct application of the block symmetric Gauss-Seidel (BSGS) method has slower convergence for smaller Knudsen numbers. Better convergence rates for dense flows are then achieved by coupling the BSGS method with the micro-macro decomposition, which treats the moment equations as a coupled system with a microscopic part and a macroscopic part. Since the macroscopic part contains only a small number of equations, it can be solved accurately during the iteration with a relatively small computational cost, which accelerates the overall iteration. The method is further generalized to the multiscale decomposition which splits the moment system into many subsystems with different orders of magnitude. Both one- and two-dimensional numerical tests are carried out to examine the performances of these methods. Possible issues regarding the efficiency and convergence are discussed in the conclusion.

**Key words.** Linearized Boltzmann equation, block symmetric Gauss-Seidel method, micro-macro decomposition, multi-scale decomposition

**1. Introduction.** Rarefied gas flows occur in various natural and engineering systems, including high-altitude atmosphere, space environments, vacuum systems and micro/nano-scale devices. Accurate description of rarefied gases requires the kinetic theory, which models the distribution of gas molecules in the position-velocity space. The Boltzmann equation, a basic kinetic model for rarefied gas dynamics covering continuum to free molecular flow regimes, takes into account molecular transport and collisions, providing an accurate representation of rarefied gas behaviors. Classical continuum fluid dynamics equations like the Euler and Navier-Stokes-Fourier equations can be derived as asymptotic limits of the Boltzmann equation when the Knudsen number, defined as the ratio of the molecular mean free path of a gas to a characteristic length scale of the flow, is small ( $\ll 1$ ) [11, 9]. However, since they become inadequate for large Knudsen number, one still needs to solve kinetic models to obtain quantitatively correct flow structures.

One major difficulty in solving the Boltzmann equation comes from its high dimensionality. Compared with continuum models, the Boltzmann equation has an additional velocity variable that is usually three-dimensional. It doubles the number of dimensions and adds a huge amount of computational cost. Many simulations require supercomputers or GPUs to get accurate results [12, 17]. The moment method, proposed by Grad [13], is one major approach to the dimensionality reduction. Grad's moment method adds balance laws of non-equilibrium quantities to the conservation laws of mass, momentum and energy. With a few more variables added to the system, the results can be significantly improved [28, 3]. Grad's moment method suffers from difficulties including the loss of hyperbolicity [22] and the convergence issue [7], but in the linear regime where the flow is close to a global equilibrium, Grad's method performs well and can be applied with many moments [25, 20], and the convergence towards the Boltzmann equation has been proven in [24]. With moment methods, we expect that simulations of two-dimensional problems can be completed on personal computers within hours or even minutes [36, 21].

Numerical methods for moment methods including 13 or 26 moments have been studied extensively in the recent two decades [35, 14, 23, 34], but there are relatively few references for many-moment methods, especially for steady-state equations. In [36], the authors used the discontinuous Galerkin method for spatial discretization, and the resulting linear system is solved by the PARDISO solver [27]. In this work, we will focus on the iterative linear solver of the steady-state equations, and we hope the method has the potential to be generalized to nonlinear equations. Since the moment method can be considered as the semidiscrete Boltzmann equation with the velocity variable discretized, ideas from the other numerical methods for the steady-state Boltzmann equation can be borrowed to design our numerical scheme. One classical iterative method to solve steady-state equations is the source iteration [1], also known as the conventional iterative scheme (CIS) [33], which has a slow convergence when the collision operator gets stiff in the case of small Knudsen numbers. By von Neumann analysis, it can be shown that the error grows in the form of  $[1 - O(\epsilon^2)]^n$

---

\*Submitted to arXiv December 11, 2023.

**Funding:** Zhenning Cai's work was supported by the Academic Research Fund of the Ministry of Education of Singapore under grant A-0008592-00-00.

<sup>†</sup>Department of Mathematics, National University of Singapore, Singapore 119076 ([xydong@nus.edu.sg](mailto:xydong@nus.edu.sg)).

<sup>‡</sup>Department of Mathematics, National University of Singapore, Singapore 119076 ([matcz@nus.edu.sg](mailto:matcz@nus.edu.sg)).

with  $\epsilon$  being the Knudsen number and  $n$  being the number of iterations. A recent improvement of the CIS is the general synthetic iterative scheme (GSIS) [32, 33], which is shown to have a uniform lower bound of the amplification factor for all Knudsen numbers  $\epsilon$ . This method is based on the micro-macro decomposition of distribution functions, and has been applied to many other cases [38, 37].

In our work, we will put forward a family of new iterative solvers based on the block symmetric Gauss-Seidel (BSGS) method. We will first show that the straightforward application of the first-order BSGS method has the convergence rate  $[1 - O(\epsilon)]^n$ , which is better than the classical CIS. To improve its performance in dense regimes, we adopt an idea similar to GSIS by coupling the BSGS method with a micro-macro decomposition of the moments. Our scheme is further generalized to second-order methods and multiscale decomposition of the moments, which results in a family of iterative schemes for the steady-state moment equations. In the rest part of this paper, we will first introduce the moment equations and its spatial discretization in Section 2, and then study the BSGS method and its convergence in Section 3. Section 4 introduces the micro-macro decomposition to the iterative method to improve the convergence rate at small Knudsen numbers, and it is further generalized by replacing the micro-macro decomposition with the multiscale decomposition. Numerical tests are carried out in Section 5 to show the performances of these methods under different parameter settings. Finally, some concluding remarks are given in Section 6.

**2. Upwind finite volume method for the linearized Boltzmann equation.** In this paper, we consider the general linearized steady-state Boltzmann equation

$$(2.1) \quad \mathbf{v} \cdot \nabla_{\mathbf{x}} f(\mathbf{x}, \mathbf{v}) = \frac{1}{\epsilon} \mathcal{L}[f](\mathbf{x}, \mathbf{v}), \quad \mathbf{x}, \mathbf{v} \in \mathbb{R}^d$$

where  $f(\mathbf{x}, \mathbf{v})$  is the distribution function of position  $\mathbf{x} = (x_1, \dots, x_d)^T$  and molecular velocity  $\mathbf{v} = (v_1, \dots, v_d)^T$ .  $\epsilon$  denotes Knudsen number and the operator  $\mathcal{L}$  represents the linearized Boltzmann collision operator.

**2.1. Linearized Boltzmann equation and moment equations.** The distribution function  $f$  in (2.1) is discretized by the spectral method, which is based on the expansion of  $f$  into an infinite series:

$$(2.2) \quad f(\mathbf{x}, \mathbf{v}) = \sum_{n=0}^{\infty} u^n(\mathbf{x}) \varphi_n(\mathbf{v}) \omega(\mathbf{v})$$

where  $\omega(\cdot)$  is the weight function, and  $\varphi_n$  stands for the basis functions satisfying

$$\int \varphi_n^*(\mathbf{v}) \varphi_{n'}(\mathbf{v}) \omega(\mathbf{v}) d\mathbf{v} \begin{cases} = 0 & \text{if } n \neq n', \\ > 0 & \text{if } n = n'. \end{cases}$$

When the basis functions  $\varphi_n(\cdot)$  are chosen as polynomials, the coefficients  $u^n$  denote the moments of the distributions function  $f$ . The moment equations of  $u^n$  can be derived as [13]

$$(2.3) \quad \sum_{i=1}^d \mathbf{A}_i \frac{\partial \mathbf{u}}{\partial x_i} = \frac{1}{\epsilon} \mathbf{L} \mathbf{u}$$

by truncating the infinite series (2.2) to  $N + 1$  terms and choosing the test functions to be  $\varphi_n$  with  $n = 0, 1, \dots, N$ . Here the unknown vector  $\mathbf{u}$  is

$$\mathbf{u} = (u^0, u^1, \dots, u^N)^T.$$

The coefficient matrices  $\mathbf{A}_i$  have real eigenvalues, and  $\mathbf{L}$  is Hermitian negative semidefinite due to the self-adjointness of the linear collision operator  $\mathcal{L}$ . When  $N$  tends to infinity, the equations (2.3) are expected to converge to the linearized Boltzmann equation (2.1).

**REMARK 1.** *In most moment methods, the weight function  $\omega(\mathbf{v})$  is chosen as  $C \exp(-|\mathbf{v}|^2/2)$  which is the Maxwellian, where  $C$  is the normalizing constant. Then, by selecting different basis functions  $\varphi_n$ , the system (2.3) will correspond to different moment equations. Examples include Grad's moment equations [13] and regularized moment equations [30].*

**2.2. Spatial discretization.** In this work, we adopt the finite volume method to discretize the moment equations (2.3). In particular, the upwind method with linear reconstruction is applied to discretize the advection term. Such a method is commonly used in computational fluid dynamics, and we will detail the one- and two-dimensional cases in the following subsections to facilitate our future discussion.

**2.2.1. One-dimensional case.** In the one-dimensional case, we assume that  $\mathbf{u}$  is homogeneous in  $x_2, \dots, x_d$ , and thus (2.3) can be simplified to

$$(2.4) \quad \mathbf{A} \frac{d\mathbf{u}}{dx} = \frac{1}{\epsilon} \mathbf{L} \mathbf{u},$$

where  $x$  and  $\mathbf{A}$  refer to  $x_1$  and  $\mathbf{A}_1$ , respectively. For simplicity, we assume that the spatial grid is uniform, and the cell size is  $\Delta x$ . Thus, using  $\bar{\mathbf{u}}_j$  to represent average  $\mathbf{u}(x)$  on the  $j$ th grid cell, the upwind method can be formulated as

$$(2.5) \quad \mathbf{A}^+ (\mathbf{u}_{j+1/2}^- - \mathbf{u}_{j-1/2}^-) + \mathbf{A}^- (\mathbf{u}_{j+1/2}^+ - \mathbf{u}_{j-1/2}^+) = \frac{1}{\epsilon} \Delta x \mathbf{L} \bar{\mathbf{u}}_j,$$

where  $\mathbf{A}^\pm$  can be obtained by diagonalization of  $\mathbf{A}$ :

$$\mathbf{A} = \mathbf{R} \mathbf{D} \mathbf{R}^{-1}, \quad |\mathbf{A}| = \mathbf{R} |\mathbf{D}| \mathbf{R}^{-1}, \quad \mathbf{A}^\pm = \frac{1}{2} (\mathbf{A} \pm |\mathbf{A}|)$$

with  $\mathbf{D} = \text{diag}(\lambda_0, \lambda_1, \dots, \lambda_N)$  and  $|\mathbf{D}| = \text{diag}(|\lambda_0|, |\lambda_1|, \dots, |\lambda_N|)$ , and  $\mathbf{u}_{j+1/2}^\pm$  are values of the numerical solution on the cell boundaries obtained by linear reconstruction. For first-order schemes,  $\mathbf{u}_{j+1/2}^- = \bar{\mathbf{u}}_j$  and  $\mathbf{u}_{j+1/2}^+ = \bar{\mathbf{u}}_{j+1}$ , so that the first-order upwind scheme turns out to be

$$(2.6) \quad -\mathbf{A}^+ \bar{\mathbf{u}}_{j-1} + \left( |\mathbf{A}| - \frac{1}{\epsilon} \Delta x \mathbf{L} \right) \bar{\mathbf{u}}_j + \mathbf{A}^- \bar{\mathbf{u}}_{j+1} = \mathbf{0}.$$

To obtain second-order schemes, we apply linear reconstructions without limiters:

$$\mathbf{u}_{j+1/2}^- = \bar{\mathbf{u}}_j + \frac{\bar{\mathbf{u}}_{j+1} - \bar{\mathbf{u}}_{j-1}}{4}, \quad \mathbf{u}_{j+1/2}^+ = \bar{\mathbf{u}}_{j+1} + \frac{\bar{\mathbf{u}}_{j+2} - \bar{\mathbf{u}}_j}{4},$$

so that the numerical scheme reads

$$(2.7) \quad \frac{1}{4} \mathbf{A}^+ \bar{\mathbf{u}}_{j-2} - \left( \frac{1}{4} \mathbf{A} + \mathbf{A}^+ \right) \bar{\mathbf{u}}_{j-1} + \left( \frac{3}{4} |\mathbf{A}| - \frac{1}{\epsilon} \Delta x \mathbf{L} \right) \bar{\mathbf{u}}_j + \left( \frac{1}{4} \mathbf{A} + \mathbf{A}^- \right) \bar{\mathbf{u}}_{j+1} - \frac{1}{4} \mathbf{A}^- \bar{\mathbf{u}}_{j+2} = \mathbf{0}.$$

**2.2.2. Two-dimensional case.** Similarly, for two-dimensional problems, we assume that the solution is homogeneous in the  $x_3, \dots, x_d$  direction, allowing us to rewrite the moment equations (2.3) as

$$\mathbf{A}_x \frac{\partial \mathbf{u}}{\partial x} + \mathbf{A}_y \frac{\partial \mathbf{u}}{\partial y} = \frac{1}{\epsilon} \mathbf{L} \mathbf{u}.$$

Again, we assume that a uniform grid with cell size  $\Delta x \times \Delta y$  is applied to discretize the spatial domain. Using  $\bar{\mathbf{u}}_{j,k}$  to represent the average of the solution in the  $(j, k)$ th grid cell, the first-order upwind scheme is

$$(2.8) \quad -\Delta y \mathbf{A}_x^+ \bar{\mathbf{u}}_{j-1,k} - \Delta x \mathbf{A}_y^+ \bar{\mathbf{u}}_{j,k-1} + \left( \Delta y |\mathbf{A}_x| + \Delta x |\mathbf{A}_y| - \frac{1}{\epsilon} \Delta x \Delta y \mathbf{L} \right) \bar{\mathbf{u}}_{j,k} + \Delta x \mathbf{A}_y^- \bar{\mathbf{u}}_{j,k+1} + \Delta y \mathbf{A}_x^- \bar{\mathbf{u}}_{j+1,k} = \mathbf{0}.$$

The second-order scheme can again be constructed by linear reconstruction without limiters:

$$(2.9) \quad \begin{aligned} & \frac{1}{4} \Delta y \mathbf{A}_x^+ \bar{\mathbf{u}}_{j-2,k} - \Delta y \left( \frac{1}{4} \mathbf{A}_x + \mathbf{A}_x^+ \right) \bar{\mathbf{u}}_{j-1,k} + \frac{1}{4} \Delta x \mathbf{A}_y^+ \bar{\mathbf{u}}_{j,k-2} - \Delta x \left( \frac{1}{4} \mathbf{A}_y + \mathbf{A}_y^+ \right) \bar{\mathbf{u}}_{j,k-1} \\ & + \left( \frac{3}{4} \Delta y |\mathbf{A}_x| + \frac{3}{4} \Delta x |\mathbf{A}_y| - \frac{1}{\epsilon} \Delta x \Delta y \mathbf{L} \right) \bar{\mathbf{u}}_{j,k} \\ & + \Delta x \left( \frac{1}{4} \mathbf{A}_y + \mathbf{A}_y^- \right) \bar{\mathbf{u}}_{j,k+1} - \frac{1}{4} \Delta x \mathbf{A}_y^- \bar{\mathbf{u}}_{j,k+2} + \Delta y \left( \frac{1}{4} \mathbf{A}_x + \mathbf{A}_x^- \right) \bar{\mathbf{u}}_{j+1,k} - \frac{1}{4} \Delta y \mathbf{A}_x^- \bar{\mathbf{u}}_{j+2,k} = \mathbf{0}. \end{aligned}$$



**3.2. Convergence analysis for the first-order BSGS method.** For simplicity, we study the convergence of the first-order BSGS method by assuming that the velocity variable  $\mathbf{v}$  is also one-dimensional (denoted by  $v$  below), so that the steady-state Boltzmann equation reads

$$(3.5) \quad v \frac{\partial f}{\partial x}(x, v) = \frac{1}{\epsilon} \mathcal{L}[f](x, v),$$

where the kernel of the linearized collision operator is

$$\ker \mathcal{L} = \text{span}\{\Phi(v)\omega(v)\},$$

where

$$(3.6) \quad \Phi(v) = (1, v, v^2 - 1), \quad \omega(v) = \frac{1}{\sqrt{2\pi}} \exp\left(-\frac{v^2}{2}\right).$$

Furthermore, we will focus on the problem without velocity discretization, so that the upwind scheme becomes

$$(3.7) \quad -v^+ \bar{f}_{j-1}(v) + \left(|v| - \frac{1}{\epsilon} \Delta x \mathcal{L}\right) \bar{f}_j(v) + v^- \bar{f}_{j+1}(v) = 0,$$

where  $v^+ = \max\{v, 0\}$ ,  $v^- = \min\{v, 0\}$ , and  $\bar{f}_j(v)$  approximates the average of  $f(x, v)$  in the  $j$ th cell. Such a simplification allows us to compute some integrals exactly and get analytical results for the convergence rate. We expect that the conclusion will also be applicable when  $N$  in the moment equations (2.3) is sufficiently large. Note that by comparing (3.7) and (2.6), one can find that  $\mathbf{A}$ ,  $\mathbf{L}$  and  $\bar{\mathbf{u}}_j$  are the discrete versions of  $v$ ,  $\mathcal{L}$  and  $\bar{f}_j$ , respectively.

The symmetric Gauss-Seidel method can be applied to (3.7) in a similar manner to the BSGS method for the moment equations. We use  $f_j^{(n+1/2)}(v)$  to denote the solution after the left-to-right sweeping and use  $f_j^{(n+1)}(v)$  to denote the solution after the right-to-left sweeping. Assume the exact solution of (3.7) is  $f_j^*(v)$ . Then the error functions

$$h_j^{(n)}(v) := f_j^{(n-1/2)}(v) - f_j^*(v), \quad e_j^{(n)}(v) := f_j^{(n)}(v) - f_j^*(v)$$

satisfy the following equations:

$$(3.8) \quad \begin{cases} -v^+ h_{j-1}^{(n+1)}(v) + \left(|v| - \frac{1}{\epsilon} \Delta x \mathcal{L}\right) h_j^{(n+1)}(v) + v^- e_{j+1}^{(n)}(v) = 0, \\ -v^+ h_{j-1}^{(n+1)}(v) + \left(|v| - \frac{1}{\epsilon} \Delta x \mathcal{L}\right) e_j^{(n+1)}(v) + v^- e_{j+1}^{(n+1)}(v) = 0. \end{cases}$$

A rigorous analysis of (3.8) requires a close look into the boundary conditions, which becomes rather involved especially when we have wall boundary conditions. Below we will take a simpler strategy and apply the Fourier analysis by assuming periodic boundary conditions. Under this assumption, the lower/upper triangular matrices used in the symmetric Gauss-Seidel method will become circulant matrices, so that the corresponding numerical method is not exactly the one used in practice. Reference [10] carried out comparison between the Fourier analysis and the classical analysis for a class of methods including the Gauss-Seidel method and the SSOR method. It is found that the two analyses provide quite similar results, although the Fourier analysis sometimes predicts a slightly slower convergence rate. Such a phenomenon is further explained in [19]. For our purposes, the Fourier analysis can already reveal sufficient insights of the problem.

Following the Fourier stability analysis, we assume

$$(3.9) \quad \begin{pmatrix} h_j^{(n)} \\ e_j^{(n)} \end{pmatrix} = \lambda^n \mathbf{w}(v) \exp(i\xi j \Delta x).$$

Substituting (3.9) into the error equations (3.8), one obtains

$$(3.10) \quad \begin{pmatrix} \lambda \left[ |v| - \frac{1}{\epsilon} \Delta x \mathcal{L} - v^+ e^{-i\eta} \right] & v^- e^{-i\eta} \\ -\lambda v^+ e^{i\eta} & \lambda \left[ |v| - \frac{1}{\epsilon} \Delta x \mathcal{L} + v^- e^{i\eta} \right] \end{pmatrix} \mathbf{w}(v) = \mathbf{0},$$

where  $\eta = \xi \Delta x$ .

On account of the obstacles of solving the Boltzmann equation for low Knudsen numbers, we are more concerned about the situations where  $\epsilon$  is small. We therefore carry out asymptotic expansions of  $\lambda$  and  $\mathbf{w}(v)$  with respect to  $\epsilon$ :

$$(3.11) \quad \lambda = \lambda_0 + \epsilon \lambda_1 + \epsilon^2 \lambda_2 + \dots, \quad \mathbf{w}(v) = \mathbf{w}_0(v) + \epsilon \mathbf{w}_1(v) + \epsilon^2 \mathbf{w}_2(v) + \dots.$$

Replacing  $\lambda$  and  $\mathbf{w}(v)$  in the equations (3.10) by the expansions (3.11), we find that the equations for the  $O(\epsilon^{-1})$ ,  $O(1)$  and  $O(\epsilon)$  terms are:

$$(3.12a) \quad \lambda_0 \begin{pmatrix} \mathcal{L} & 0 \\ 0 & \mathcal{L} \end{pmatrix} \mathbf{w}_0(v) = \mathbf{0},$$

$$(3.12b) \quad \begin{pmatrix} \lambda_0 (|v| - e^{-i\eta} v^+) & e^{i\eta} v^- \\ -\lambda_0 e^{-i\eta} v^+ & \lambda_0 (|v| + e^{i\eta} v^-) \end{pmatrix} \mathbf{w}_0(v) = \Delta x \begin{pmatrix} \mathcal{L} & 0 \\ 0 & \mathcal{L} \end{pmatrix} [\lambda_0 \mathbf{w}_1(v) + \lambda_1 \mathbf{w}_0(v)],$$

$$(3.12c) \quad \begin{pmatrix} \lambda_0 (|v| - e^{-i\eta} v^+) & e^{i\eta} v^- \\ -\lambda_0 e^{-i\eta} v^+ & \lambda_0 (|v| + e^{i\eta} v^-) \end{pmatrix} \mathbf{w}_1(v) \\ + \begin{pmatrix} \lambda_1 (|v| - e^{-i\eta} v^+) & 0 \\ -\lambda_1 e^{-i\eta} v^+ & \lambda_1 (|v| + e^{i\eta} v^-) \end{pmatrix} \mathbf{w}_0(v) = \Delta x \begin{pmatrix} \mathcal{L} & 0 \\ 0 & \mathcal{L} \end{pmatrix} [\lambda_0 \mathbf{w}_2(v) + \lambda_1 \mathbf{w}_1(v) + \lambda_2 \mathbf{w}_0(v)].$$

The theorem below states properties of  $\lambda_0$ :

**THEOREM 3.1.** *Let  $\eta \in (0, 2\pi)$  and  $\Delta x > 0$ . Assume that  $\lambda_0$ ,  $\lambda_1$  and  $\mathbf{w}_0(v)$ ,  $\mathbf{w}_1(v)$ ,  $\mathbf{w}_2(v)$  satisfy (3.12) for any  $v \in \mathbb{R}$ , and  $\mathbf{w}_0(v)$  is a nonzero function. Then it holds that  $|\lambda_0| \leq 1/(5 - 4 \cos(\eta))$ . The maximum value is attained when  $\lambda_0 = 1/(5 - 4 \cos(\eta))$ .*

*Proof.* If  $\lambda_0 = 0$ , it clearly satisfies  $|\lambda_0| \leq 1/(5 - 4 \cos(\eta))$ . We will thus focus on the case where  $\lambda_0$  is nonzero. According to (3.12a), both components of  $\mathbf{w}_0$  must be in the kernel of the linearized collision operator  $\mathcal{L}$ , and therefore there exist  $\boldsymbol{\alpha} = (\alpha_0, \alpha_1, \alpha_2)^T$  and  $\boldsymbol{\beta} = (\beta_0, \beta_1, \beta_2)^T$  satisfying

$$(3.13) \quad \mathbf{w}_0(v) = \begin{pmatrix} \Phi(v) \\ \Phi(v) \end{pmatrix} \begin{pmatrix} \boldsymbol{\alpha} \\ \boldsymbol{\beta} \end{pmatrix} \omega(v),$$

where  $\Phi$  is defined in (3.6). Left-multiplying both sides of (3.12b) by  $\begin{pmatrix} \Phi^*(v) \\ \Phi^*(v) \end{pmatrix}$  and integrating the result with respect to  $v$ , we can obtain by the conservation properties of the collision operator that

$$(3.14) \quad \mathbf{Q} \begin{pmatrix} \boldsymbol{\alpha} \\ \boldsymbol{\beta} \end{pmatrix} = \mathbf{0}$$

where

$$(3.15) \quad \mathbf{Q} = \frac{1}{\sqrt{2\pi}} \begin{pmatrix} \lambda_0(2 - e^{-i\eta}) & -\lambda_0 \sqrt{\frac{\pi}{2}} e^{-i\eta} & \lambda_0(2 - e^{-i\eta}) & -e^{i\eta} & \sqrt{\frac{\pi}{2}} e^{i\eta} & -e^{i\eta} \\ -\lambda_0 \sqrt{\frac{\pi}{2}} e^{-i\eta} & 2\lambda_0(2 - e^{-i\eta}) & -\lambda_0 \sqrt{2\pi} e^{-i\eta} & \sqrt{\frac{\pi}{2}} e^{i\eta} & -2e^{i\eta} & \sqrt{2\pi} e^{i\eta} \\ \lambda_0(2 - e^{-i\eta}) & -\lambda_0 \sqrt{2\pi} e^{-i\eta} & 5\lambda_0(2 - e^{-i\eta}) & -e^{i\eta} & \sqrt{2\pi} e^{i\eta} & -5e^{i\eta} \\ -\lambda_0 e^{-i\eta} & -\lambda_0 \sqrt{\frac{\pi}{2}} e^{-i\eta} & -\lambda_0 e^{-i\eta} & \lambda_0(2 - e^{i\eta}) & \lambda_0 \sqrt{\frac{\pi}{2}} e^{i\eta} & \lambda_0(2 - e^{i\eta}) \\ -\lambda_0 \sqrt{\frac{\pi}{2}} e^{-i\eta} & -2\lambda_0 e^{-i\eta} & -\lambda_0 \sqrt{2\pi} e^{-i\eta} & \lambda_0 \sqrt{\frac{\pi}{2}} e^{i\eta} & 2\lambda_0(2 - e^{i\eta}) & \lambda_0 \sqrt{2\pi} e^{i\eta} \\ -\lambda_0 e^{-i\eta} & -\lambda_0 \sqrt{2\pi} e^{-i\eta} & -5\lambda_0 e^{-i\eta} & \lambda_0(2 - e^{i\eta}) & \lambda_0 \sqrt{2\pi} e^{i\eta} & 5\lambda_0(2 - e^{i\eta}) \end{pmatrix}.$$

Since  $\mathbf{w}_0$  is nonzero, the vector  $\boldsymbol{\alpha}$  and  $\boldsymbol{\beta}$  cannot be both zero vectors. Thus, in (3.14), the matrix  $\mathbf{Q}$  must be singular, *i.e.*  $\det(\mathbf{Q}) = 0$ . This gives a sextic equation of  $\lambda_0$ . The equation has four real roots:

$$\lambda_0^{(1)} = \frac{1}{5 - 4 \cos(\eta)}, \quad \lambda_0^{(2,3,4)} = 0.$$

The other two complex roots satisfy

$$\begin{aligned} |\lambda_0^{(5)}| = |\lambda_0^{(6)}| &= \frac{16 - 5\pi}{\sqrt{(16 - 5\pi)^2 + 128(16 + 15\pi)(1 - \cos(\eta)) + 256(16 - 5\pi)(1 - \cos(\eta))^2}} \\ &< \frac{16 - 5\pi}{\sqrt{(16 - 5\pi)^2 + 8(16 - 5\pi)^2(1 - \cos(\eta)) + 16(16 - 5\pi)^2(1 - \cos(\eta))^2}} = |\lambda_0^{(1)}|. \end{aligned}$$

This confirms that  $\lambda_0 \leq 1/(5 - 4 \cos(\eta))$ , and the maximum value is attained if  $\lambda_0 = \lambda_0^{(1)}$ .  $\square$

Note that this estimation of  $\lambda_0$  holds for any collision operators. If the collision operator  $\mathcal{L}$  is the linearized BGK operator defined by

$$(3.16) \quad \mathcal{L}[f](x, v) = \mathcal{M}[f](x, v) - f(x, v)$$

with

$$(3.17) \quad \mathcal{M}[f](v) = \left[ \int_{\mathbb{R}} \Phi(v) f(v) dv \right] \begin{pmatrix} 1 \\ v \\ (v^2 - 1)/2 \end{pmatrix} \omega(v),$$

then  $\lambda_1$  can also be computed:

**THEOREM 3.2.** *Let  $\eta \in (0, 2\pi)$  and  $\Delta x > 0$ . Assume that  $\lambda_0, \lambda_1$  and  $\mathbf{w}_0(v), \mathbf{w}_1(v), \mathbf{w}_2(v)$  satisfy (3.12) with  $\mathcal{L}$  defined by (3.16), and  $\mathbf{w}_0(v)$  is a nonzero function. If  $\lambda_0 = 1/(5 - 4 \cos(\eta))$ , then*

$$(3.18) \quad \lambda_1 = -\frac{36\sqrt{2\pi}[1 - \cos(\eta)]}{5\Delta x[5 - 4 \cos(\eta)]^2} < 0.$$

*Proof.* When  $\lambda_0 = 1/(5 - 4 \cos(\eta))$ , the function  $\mathbf{w}_0(v)$  given by (3.13) can be obtained by solving (3.14). The result is

$$(3.19) \quad \mathbf{w}_0(v) = \begin{pmatrix} e^{i\eta}(2 - e^{i\eta}) \\ 1 \end{pmatrix} (v^2 - 3) \omega(v).$$

To obtain  $\lambda_1$ , we take moments of (3.12c) to get

$$(3.20) \quad \int_{-\infty}^{\infty} \begin{pmatrix} \Phi^*(v) \\ \Phi^*(v) \end{pmatrix} \left[ \begin{pmatrix} \lambda_0(|v| - e^{-i\eta}v^+) & e^{i\eta}v^- \\ -\lambda_0 e^{-i\eta}v^+ & \lambda_0(|v| + e^{i\eta}v^-) \end{pmatrix} \mathbf{w}_1(v) \right. \\ \left. + \begin{pmatrix} \lambda_1(|v| - e^{-i\eta}v^+) & 0 \\ -\lambda_1 e^{-i\eta}v^+ & \lambda_1(|v| + e^{i\eta}v^-) \end{pmatrix} \mathbf{w}_0(v) \right] \omega(v) dv = \mathbf{0}.$$

Since  $\mathcal{L}$  is the BGK collision operator defined by (3.16), the first-order term  $\mathbf{w}_1(v)$  can be decomposed into  $\mathbf{w}_1(v) = \mathbf{w}_{10}(v) + \mathbf{w}_{11}(v)$ , where

$$(3.21) \quad \mathbf{w}_{11}(v) = -\begin{pmatrix} \mathcal{L} & 0 \\ 0 & \mathcal{L} \end{pmatrix} \mathbf{w}_1(v),$$

and  $\mathbf{w}_{10}(v)$  has the form

$$\mathbf{w}_{10} = \begin{pmatrix} \Phi(v) \\ \Phi(v) \end{pmatrix} \begin{pmatrix} \gamma \\ \tau \end{pmatrix} \omega(v)$$

with  $\gamma = (\gamma_0, \gamma_1, \gamma_2)^T$ ,  $\tau = (\tau_0, \tau_1, \tau_2)^T$ . Plugging (3.21) into (3.12b) yields

$$\begin{pmatrix} \lambda_0(|v| - e^{-i\eta}v^+) & e^{i\eta}v^- \\ -\lambda_0 e^{-i\eta}v^+ & \lambda_0(|v| + e^{i\eta}v^-) \end{pmatrix} \mathbf{w}_0(v) = -\Delta x \lambda_0 \mathbf{w}_{11}(v),$$

which allows us to express  $\mathbf{w}_{11}(v)$  using  $\mathbf{w}_0(v)$ , so that  $\mathbf{w}_1(v)$  can be expressed using  $\mathbf{w}_{10}(v)$  and  $\mathbf{w}_0(v)$ :

$$\mathbf{w}_1(v) = \begin{pmatrix} \Phi(v) \\ \Phi(v) \end{pmatrix} \begin{pmatrix} \gamma \\ \tau \end{pmatrix} \omega(v) - \frac{1}{\lambda_0 \Delta x} \begin{pmatrix} \lambda_0(|v| - e^{-i\eta}v^+) & e^{i\eta}v^- \\ -\lambda_0 e^{-i\eta}v^+ & \lambda_0(|v| + e^{i\eta}v^-) \end{pmatrix} \mathbf{w}_0(v),$$

so that (3.20) can be rewritten as

$$(3.22) \quad \mathbf{Q} \begin{pmatrix} \gamma \\ \tau \end{pmatrix} = \int_{-\infty}^{\infty} \begin{pmatrix} \Phi^*(v) \\ \Phi^*(v) \end{pmatrix} \left[ \frac{1}{\Delta x} \begin{pmatrix} \lambda_0 [|v|^2 - (2e^{-i\eta} - e^{-2i\eta})(v^+)^2] & -(2e^{i\eta} - e^{2i\eta})(v^-)^2 \\ -\lambda_0 (2e^{-i\eta} - e^{-2i\eta})(v^+)^2 & \lambda_0 [|v|^2 - (2e^{i\eta} - e^{2i\eta})(v^-)^2] \end{pmatrix} \right. \\ \left. - \begin{pmatrix} \lambda_1 (|v| - e^{-i\eta}v^+) & 0 \\ -\lambda_1 e^{-i\eta}v^+ & \lambda_1 (|v| + e^{i\eta}v^-) \end{pmatrix} \right] \mathbf{w}_0(v) dv,$$

where the matrix  $\mathbf{Q}$  has been defined in (3.15). Since  $\mathbf{Q}$  is singular, we can find its left eigenvector  $\ell = (2, 0, -1, -2(1 - 2e^{i\eta}), 0, 1 - 2e^{i\eta})$  satisfying  $\ell \mathbf{Q} = 0$ . Left-multiplying both sides of (3.22) by  $\ell$  turns the left-hand side to zero, and the right-hand side can be directly integrated by (3.19). The result is

$$\frac{5\lambda_1 \Delta x (e^{-i\eta} - 2)^2 (e^{i\eta} - 2)^2 + 18\sqrt{2\pi} (e^{-i\eta} - 1)(e^{i\eta} - 1)}{2\pi e^{-i\eta} (e^{-i\eta} - 2)(e^{i\eta} - 2)} = 0,$$

from which  $\lambda_1$  can be solved and the result is (3.18).  $\square$

These two theorems indicate that the amplification factor of the BSGS iteration is  $1/[5 - 4 \cos(\Delta x)] + O(\epsilon)$ , attained when  $\xi = 1$  or  $N - 1$ . Compared with the conventional iterative scheme, this factor does not tend to 1 as  $\epsilon$  approaches zero. Note that this factor does tend to 1 as  $\Delta x$  approaches zero. This is the typical behavior of the classical iterative methods and can usually be fixed by applying the multigrid method. This has not implemented and will be explored in our future work.

In the case of BGK collisions, we do see a slowdown of the convergence when  $\epsilon$  gets smaller, since  $\lambda_1$  can be bounded by

$$\lambda_1 \leq -\frac{36\sqrt{2\pi}(1 - \cos(\Delta x))}{5\Delta x[5 - 4 \cos(\Delta x)]^2} \approx -\frac{18}{5}\sqrt{2\pi}\Delta x.$$

We are going to tackle this problem in Sections 4. Here we first extend our method to second order via linear reconstruction.

**3.3. Block symmetric successive relaxation method for the second-order scheme.** For the second-order scheme (2.7), a direct application of the BSGS method may cause divergence (see Figure 7 in our numerical tests). One possible reason is that the reconstruction destroys the structure similar to diagonally dominant matrices, which guarantees the convergence of the Gauss-Seidel method. We therefore tweak the original method by adding a diagonal term  $\alpha|\mathbf{A}|(\bar{\mathbf{u}}_j^{(n+1/2)} - \bar{\mathbf{u}}_j^{(n)})$  (or  $\alpha|\mathbf{A}|(\bar{\mathbf{u}}_j^{(n+1)} - \bar{\mathbf{u}}_j^{(n+1/2)})$  during the backward iteration), so that the iteration becomes

$$\frac{1}{4}\mathbf{A}^+\bar{\mathbf{u}}_{j-2}^{(n+1/2)} - \left(\frac{1}{4}\mathbf{A} + \mathbf{A}^+\right)\bar{\mathbf{u}}_{j-1}^{(n+1/2)} + \mathbf{S}_\alpha\bar{\mathbf{u}}_j^{(n+1/2)} + \left(\frac{1}{4}\mathbf{A} + \mathbf{A}^-\right)\bar{\mathbf{u}}_{j+1}^{(n)} - \frac{1}{4}\mathbf{A}^-\bar{\mathbf{u}}_{j+2}^{(n)} = \alpha|\mathbf{A}|\bar{\mathbf{u}}_j^{(n)}, \\ \frac{1}{4}\mathbf{A}^+\bar{\mathbf{u}}_{j-2}^{(n+1/2)} - \left(\frac{1}{4}\mathbf{A} + \mathbf{A}^+\right)\bar{\mathbf{u}}_{j-1}^{(n+1/2)} + \mathbf{S}_\alpha\bar{\mathbf{u}}_j^{(n+1)} + \left(\frac{1}{4}\mathbf{A} + \mathbf{A}^-\right)\bar{\mathbf{u}}_{j+1}^{(n+1)} - \frac{1}{4}\mathbf{A}^-\bar{\mathbf{u}}_{j+2}^{(n+1)} = \alpha|\mathbf{A}|\bar{\mathbf{u}}_j^{(n+1/2)},$$

where

$$\mathbf{S}_\alpha = \frac{3}{4}|\mathbf{A}| - \frac{1}{\epsilon}\Delta x \mathbf{L} + \alpha|\mathbf{A}|.$$

These equations are to replace steps (2) and (3) in the algorithm introduced in Section 3.1. In most of our test cases, we choose  $\alpha = 1/4$ , which is sufficient to recover the convergence of the iteration. For conciseness, we call this method the block symmetric successive relaxation (BSSR) method.

**4. Coupling with the micro-macro decomposition.** To improve the convergence rate in the case of low Knudsen numbers, we try to improve the iterative method using the micro-macro decomposition [4]. Below we will mainly study the coupling of the first-order BSGS method and the micro-macro decomposition for the one-dimensional Boltzmann equation (3.5). The idea can be naturally generalized to the multi-dimensional BSSR method.

**4.1. BSGS method with micro-macro decomposition.** To implement the micro-macro decomposition, we set the weight function  $\omega(v)$  to be the Maxwellian (3.6) and choose basis functions such that  $(\varphi_0(v), \varphi_1(v), \varphi_2(v)) = \Phi(v)$ . Thus, the coefficients  $\mathbf{u}$  can be split into equilibrium and non-equilibrium variables:

$$\mathbf{u}_*^1 = (u^0, u^1, u^2)^T, \quad \mathbf{u}_*^2 = (u^3, \dots, u^N)^T.$$

Thus, the linear system (2.4) can be written as

$$(4.1) \quad \begin{cases} \mathbf{A}_{11}^* \frac{d\mathbf{u}_*^1}{dx} + \mathbf{A}_{12}^* \frac{d\mathbf{u}_*^2}{dx} = \mathbf{0}, \\ \mathbf{A}_{21}^* \frac{d\mathbf{u}_*^1}{dx} + \mathbf{A}_{22}^* \frac{d\mathbf{u}_*^2}{dx} = \frac{1}{\epsilon} \mathbf{L}_{22}^* \mathbf{u}_*^2 \end{cases}$$

where  $\mathbf{L}_{22}^*$  is an  $(N-2) \times (N-2)$  matrix representing the collision term, and

$$\mathbf{A}_{11}^* = \begin{pmatrix} 0 & 1 & 0 \\ 1 & 0 & 2 \\ 0 & 1 & 0 \end{pmatrix}.$$

The idea of the micro-macro decomposition is to solve the two equations in (4.1) alternately. We first assume  $\mathbf{u}_*^2$  is given and solve  $\mathbf{u}_*^1$  from the first equation, and then plug the result into the second equation to solve  $\mathbf{u}_*^2$ , which completes one iteration. However, for fixed  $\mathbf{u}_*^2$ , the first equation of (4.1) may not admit a solution since for  $\mathbf{v} = (1, 0, -1)^T$ ,

$$\mathbf{v}^T \left( \mathbf{A}_{11}^* \frac{d\mathbf{u}_*^1}{dx} + \mathbf{A}_{12}^* \frac{d\mathbf{u}_*^2}{dx} \right) = \mathbf{v}^T \mathbf{A}_{12}^* \frac{d\mathbf{u}_*^2}{dx},$$

which may not be zero for the given  $\mathbf{u}_*^2$ . Our solution is to include a few more coefficients in the first part to guarantee the solvability of both equations. In general, we assume

$$(4.2) \quad \mathbf{u}^1 = (u^0, u^1, u^2, \dots, u^{N_0})^T, \quad \mathbf{u}^2 = (u^{N_0+1}, \dots, u^N)^T,$$

which satisfy the linear system

$$(4.3) \quad \begin{cases} \mathbf{A}_{11} \frac{d\mathbf{u}^1}{dx} + \mathbf{A}_{12} \frac{d\mathbf{u}^2}{dx} = \frac{1}{\epsilon} (\mathbf{L}_{11} \mathbf{u}^1 + \mathbf{L}_{12} \mathbf{u}^2), \\ \mathbf{A}_{21} \frac{d\mathbf{u}^1}{dx} + \mathbf{A}_{22} \frac{d\mathbf{u}^2}{dx} = \frac{1}{\epsilon} (\mathbf{L}_{21} \mathbf{u}^1 + \mathbf{L}_{22} \mathbf{u}^2). \end{cases}$$

In practice, choosing  $N_0 = 3$  usually suffices to allow iterating between  $\mathbf{u}^1$  and  $\mathbf{u}^2$  smoothly.

In general, it is unnecessary to solve  $\mathbf{u}^1$  and  $\mathbf{u}^2$  exactly during the inner iteration. Since the equation of  $\mathbf{u}^1$  contains only a small number of unknowns, below we will assume that the first equation of (4.3) is accurately solved but only one BSGS iteration is applied to the second equation. We call this approach the BSGS-MM (BSGS with micro-macro decomposition) method. To apply it to the upwind scheme (2.5), we define the following block structures for the matrices  $\mathbf{A}^\pm$  and  $|\mathbf{A}|$ :

$$\mathbf{A}^\pm = \begin{pmatrix} \mathbf{A}_{11}^\pm & \mathbf{A}_{12}^\pm \\ \mathbf{A}_{21}^\pm & \mathbf{A}_{22}^\pm \end{pmatrix}, \quad |\mathbf{A}| = \begin{pmatrix} |\mathbf{A}_{11}| & |\mathbf{A}_{12}| \\ |\mathbf{A}_{21}| & |\mathbf{A}_{22}| \end{pmatrix}.$$

Note that here  $\mathbf{A}_{ij}^\pm$  is defined as a block of  $\mathbf{A}^\pm$ , which may not be the positive/negative part of  $\mathbf{A}_{ij}$  based on the eigendecomposition. The detail of the BSGS-MM method is given below:

- (1) Set the error tolerance  $tol$  and the maximum number of iterations. Set  $n = 0$  and prepare the initial values  $\bar{\mathbf{u}}_j^{1,(0)}$  and  $\bar{\mathbf{u}}_j^{2,(0)}$  for  $j = 1, \dots, M$  satisfying (3.2).
- (2) Solve  $\bar{\mathbf{u}}_j^{1,(n+1)}$  for all  $j = 1, 2, \dots, M$  by

$$(4.4) \quad \begin{aligned} -\mathbf{A}_{11}^+ \bar{\mathbf{u}}_{j-1}^{1,(n+1)} + \left( |\mathbf{A}_{11}| - \frac{1}{\epsilon} \Delta x \mathbf{L}_{11} \right) \bar{\mathbf{u}}_j^{1,(n+1)} + \mathbf{A}_{11}^- \bar{\mathbf{u}}_{j+1}^{1,(n+1)} \\ = \mathbf{A}_{12}^+ \bar{\mathbf{u}}_{j-1}^{2,(n)} - \left( |\mathbf{A}_{12}| - \frac{1}{\epsilon} \Delta x \mathbf{L}_{12} \right) \bar{\mathbf{u}}_j^{2,(n)} - \mathbf{A}_{12}^- \bar{\mathbf{u}}_{j+1}^{2,(n)}, \end{aligned}$$

where  $\bar{\mathbf{u}}_0^{(\cdot)}$  and  $\bar{\mathbf{u}}_{M+1}^{(\cdot)}$  are based on the boundary conditions. Use the normalizing condition (3.2) if necessary.

- (3) Calculate  $\bar{\mathbf{u}}_j^{2,(n+1/2)}$ ,  $j = 1, 2, \dots, M$  sequentially by

$$(4.5) \quad \begin{aligned} & -\mathbf{A}_{21}^+ \bar{\mathbf{u}}_{j-1}^{1,(n+1)} + \left( |\mathbf{A}_{21}| - \frac{1}{\epsilon} \Delta x \mathbf{L}_{21} \right) \bar{\mathbf{u}}_j^{1,(n+1)} + \mathbf{A}_{21}^- \bar{\mathbf{u}}_{j+1}^{1,(n+1)} \\ & = \mathbf{A}_{22}^+ \bar{\mathbf{u}}_{j-1}^{2,(n+1/2)} - \left( |\mathbf{A}_{22}| - \frac{1}{\epsilon} \Delta x \mathbf{L}_{22} \right) \bar{\mathbf{u}}_j^{2,(n+1/2)} - \mathbf{A}_{22}^- \bar{\mathbf{u}}_{j+1}^{2,(n)} \end{aligned}$$

where  $\bar{\mathbf{u}}_0^{(\cdot)}$  and  $\bar{\mathbf{u}}_{M+1}^{(\cdot)}$  are based on the boundary conditions.

- (4) Calculate  $\bar{\mathbf{u}}_j^{2,(n+1)}$ ,  $j = 1, 2, \dots, M$  in reverse order, that is to say,  $j = M, M-1, \dots, 2, 1$  by

$$(4.6) \quad \begin{aligned} & -\mathbf{A}_{21}^+ \bar{\mathbf{u}}_{j-1}^{1,(n+1)} + \left( |\mathbf{A}_{21}| - \frac{1}{\epsilon} \Delta x \mathbf{L}_{21} \right) \bar{\mathbf{u}}_j^{1,(n+1)} + \mathbf{A}_{21}^- \bar{\mathbf{u}}_{j+1}^{1,(n+1)} \\ & = \mathbf{A}_{22}^+ \bar{\mathbf{u}}_{j-1}^{2,(n+1/2)} - \left( |\mathbf{A}_{22}| - \frac{1}{\epsilon} \Delta x \mathbf{L}_{22} \right) \bar{\mathbf{u}}_j^{2,(n+1)} - \mathbf{A}_{22}^- \bar{\mathbf{u}}_{j+1}^{2,(n+1)} \end{aligned}$$

where  $\bar{\mathbf{u}}_0^{(\cdot)}$  and  $\bar{\mathbf{u}}_{M+1}^{(\cdot)}$  are based on the boundary conditions.

- (5) Compute the residual of the equations (3.1) for  $\bar{\mathbf{u}}_j = \bar{\mathbf{u}}_j^{(n+1)}$ ,  $j = 1, \dots, M$ . Stop if the norm of the residual is less than  $tol$ . Otherwise, check if  $n > N_s$ . If not, increase  $n$  by 1 and return to step (2). Otherwise, print warning messages about the failure of convergence and stop.

In step (2), the linear system (4.4) can be solved either directly or iteratively, depending on the size of the problem. When (4.4) is solved iteratively, the tolerance of the residual should be slightly lower than  $tol$  to ensure that the final stopping criterion in step (5) can be achieved. Extension to the second-order BSSR method is straightforward. One just needs to add the correction terms from the linear reconstruction to all the equations in steps (2)(3) and (4), and add the relaxation term to the equations in steps (3) and (4). This will be referred to as BSSR-MM method hereafter. We can also get the three-dimensional BSGS-MM or BSSR-MM method by including all the five conservative quantities as well as a few non-equilibrium variables in  $\mathbf{u}_1$  to guarantee the solvability of the equations.

Intuitively, when  $\epsilon$  is small, the conservative variables included in  $\mathbf{u}^1$  contains major information of the distribution function, so that solving (4.4) exactly already provides a good approximation of the exact solution. This will be demonstrated via convergence analysis in the following subsection.

**4.2. Convergence analysis.** The convergence of the BSGS-MM method is analyzed in a similar manner to that of the BSGS method in 3.2. Here we need to split the distribution function into two parts representing  $\mathbf{u}^1$  and  $\mathbf{u}^2$ :

$$f(x, v) = f^1(x, v) + f^2(x, v),$$

with  $f^1 = \mathcal{P}f$  and  $f^2 = (\mathcal{I} - \mathcal{P})f$ , where  $\mathcal{I}$  is the identity operator, and the projection operator  $\mathcal{P}$  is defined by

$$\mathcal{P}f(x, v) = \sum_{n=0}^{N_0} \left( \int_{\mathbb{R}} |\varphi_n(v)|^2 \omega(v) dv \right)^{-1} \left( \int_{\mathbb{R}} \varphi_n(v) f(x, v) dv \right) \varphi_n(v).$$

The collision operator  $\mathcal{L}$  can be split similarly into the following two operators:

$$\mathcal{L}_1 = \mathcal{P}\mathcal{L}, \quad \mathcal{L}_2 = (\mathcal{I} - \mathcal{P})\mathcal{L}.$$

Additionally, we define the operators  $\mathcal{V}_{1,2}^\pm$  and  $|\mathcal{V}_{1,2}|$  by

$$\mathcal{V}_1^\pm f = \mathcal{P}(v^\pm f), \quad \mathcal{V}_2^\pm f = (\mathcal{I} - \mathcal{P})(v^\pm f), \quad |\mathcal{V}_1| = \mathcal{V}_1^+ - \mathcal{V}_1^-, \quad |\mathcal{V}_2| = \mathcal{V}_2^+ - \mathcal{V}_2^-.$$

Thus, the BSGS-MM method without discretization of  $v$  can be written as

$$(4.7) \quad \left\{ \begin{array}{l} -\mathcal{V}_1^+ \bar{f}_{j-1}^{1,(n+1)}(v) + \left( |\mathcal{V}_1| - \frac{1}{\epsilon} \Delta x \mathcal{L}_1 \right) \bar{f}_j^{1,(n+1)}(v) + \mathcal{V}_1^- \bar{f}_{j+1}^{1,(n+1)}(v) \\ \qquad \qquad \qquad = \mathcal{V}_1^+ \bar{f}_{j-1}^{2,(n)}(v) - |\mathcal{V}_1| \bar{f}_j^{2,(n)}(v) - \mathcal{V}_1^- \bar{f}_{j+1}^{2,(n)}(v), \\ -\mathcal{V}_2^+ \bar{f}_{j-1}^{1,(n+1)}(v) + |\mathcal{V}_2| \bar{f}_j^{1,(n+1)}(v) + \mathcal{V}_2^- \bar{f}_{j+1}^{1,(n+1)}(v) \\ \qquad \qquad \qquad = \mathcal{V}_2^+ \bar{f}_{j-1}^{2,(n+1/2)}(v) - \left( |\mathcal{V}_2| - \frac{1}{\epsilon} \Delta x \mathcal{L}_2 \right) \bar{f}_j^{2,(n+1/2)}(v) - \mathcal{V}_2^- \bar{f}_{j+1}^{2,(n)}(v), \\ -\mathcal{V}_2^+ \bar{f}_{j-1}^{1,(n+1)}(v) + |\mathcal{V}_2| \bar{f}_j^{1,(n+1)}(v) + \mathcal{V}_2^- \bar{f}_{j+1}^{1,(n+1)}(v) \\ \qquad \qquad \qquad = \mathcal{V}_2^+ \bar{f}_{j-1}^{2,(n+1/2)}(v) - \left( |\mathcal{V}_2| - \frac{1}{\epsilon} \Delta x \mathcal{L}_2 \right) \bar{f}_j^{2,(n+1)}(v) - \mathcal{V}_2^- \bar{f}_{j+1}^{2,(n+1)}(v). \end{array} \right.$$

Mimicking the analysis of the BSGS method, we let  $f_j^*(v)$  be the exact solution of (3.7) and define the error functions

$$e_j^{1,(n)}(v) = \bar{f}_j^{1,(n)}(v) - \mathcal{P} f_j^*(v), \quad h_j^{2,(n)} = \bar{f}_j^{2,(n-1/2)} - (\mathcal{I} - \mathcal{P}) f_j^*, \quad e_j^{2,(n)}(v) = \bar{f}_j^{2,(n)}(v) - (\mathcal{I} - \mathcal{P}) f_j^*(v).$$

Then the evolution of the error functions can be immediately obtained by replacing the solutions in (4.7) with the corresponding error functions. Note that the solution of  $\bar{f}_j^1(v)$  at the current time step (the  $n$ th step) never appears in (4.7). We can regard  $\bar{f}_j^{1,(n)}$  as an auxiliary variable and consider (4.7) as an iterative scheme for  $\bar{f}_j^2(v)$ . We now apply the Fourier analysis by assuming that

$$\begin{pmatrix} h_j^{2,(n)}(v) \\ e_j^{2,(n)}(v) \end{pmatrix} = \lambda^n \begin{pmatrix} \eta^2(v) \\ \varepsilon^2(v) \end{pmatrix} \exp(i\xi j \Delta x),$$

and  $\eta^2(v)$  and  $\varepsilon^2(v)$  cannot be both zero. It is not difficult to see that  $e_j^{1,(n+1)}$  also has the form  $e_j^{1,(n+1)}(v) = \lambda^n \varepsilon^1(v) \exp(i\xi j \Delta x)$ , and the functions  $\varepsilon^1(v)$ ,  $\eta^2(v)$  and  $\varepsilon^2(v)$  satisfy

$$(4.8) \quad \begin{pmatrix} -\mathcal{V}_1^+ e^{-i\eta} + |\mathcal{V}_1| + \mathcal{V}_1^- e^{i\eta} - \frac{\Delta x}{\epsilon} \mathcal{L}_1 & 0 & -\mathcal{V}_1^+ e^{-i\eta} + |\mathcal{V}_1| + \mathcal{V}_1^- e^{i\eta} \\ -\mathcal{V}_2^+ e^{-i\eta} + |\mathcal{V}_2| + \mathcal{V}_2^- e^{i\eta} & -\lambda (\mathcal{V}_2^+ e^{-i\eta} - |\mathcal{V}_2| + \frac{\Delta x}{\epsilon} \mathcal{L}_2) & \mathcal{V}_2^- e^{i\eta} \\ -\mathcal{V}_2^+ e^{-i\eta} + |\mathcal{V}_2| + \mathcal{V}_2^- e^{i\eta} & -\lambda \mathcal{V}_2^+ e^{-i\eta} & \lambda (|\mathcal{V}_2| + \mathcal{V}_2^- e^{i\eta} - \frac{\Delta x}{\epsilon} \mathcal{L}_2) \end{pmatrix} \begin{pmatrix} \varepsilon^1(v) \\ \eta^2(v) \\ \varepsilon^2(v) \end{pmatrix} = \mathbf{0},$$

where we have again used  $\eta = \xi \Delta x$  for conciseness. When  $\epsilon$  is small, the leading-order term is

$$\mathcal{L}_1 \varepsilon_0^1(v) = 0, \quad \lambda_0 \mathcal{L}_2 \eta_0^2(v) = 0, \quad \lambda_0 \mathcal{L}_2 \varepsilon_0^2(v) = 0.$$

Since the linear collision operator is negative semidefinite with the null space  $\ker \mathcal{L} = \text{span}\{\Phi \omega\} \subset \text{Ran } \mathcal{P}$ , the operator  $\mathcal{L}_2$  is negative definite on  $\text{Ran}(\mathcal{I} - \mathcal{P})$ , so that  $\lambda_0 = 0$ , indicating fast convergence for small values of  $\epsilon$ .

However, when  $\epsilon$  is large, the convergence of the BSGS-MM method may be slow. To demonstrate this, we solve (4.8) numerically for difference values of  $\epsilon$  and  $\eta$ . The results for the linearized BGK collision operator are plotted in Figure 1. It is clear that when  $\epsilon$  tends to zero, the spectral radius also tends to zero since  $\mathbf{u}^2$  is nearly zero, and  $\mathbf{u}^1$  is solved exactly during the iteration. In the next section, we will consider some extensions of the BSGS-MM method to mitigate the convergence problem with larger values of  $\epsilon$ .

**4.3. Variations of the BSGS-MM method.** According to the convergence analysis, we have learned that the BSGS-MM method may converge slowly in the rarefied regime. In this section, we consider approaches that can improve the convergence. Again, we will focus only on the improvements of the BSGS-MM method, and the extension to the BSSR-MM method is again straightforward.

**4.3.1. The Hybrid BSGS-MM method.** It has been shown that the original BSGS method and the BSGS-MM method converge fast in exactly opposite regimes. Therefore, it is natural to consider hybridizing the two methods to cover the entire range of  $\epsilon$ . Here we propose to add a  $N_b$  BSGS iterations after each BSGS-MM iteration. For simplicity, we use  $\mathcal{T}_{\text{BSGS}}$  and  $\mathcal{T}_{\text{BSGS-MM}}$  to denote the iteration operators for

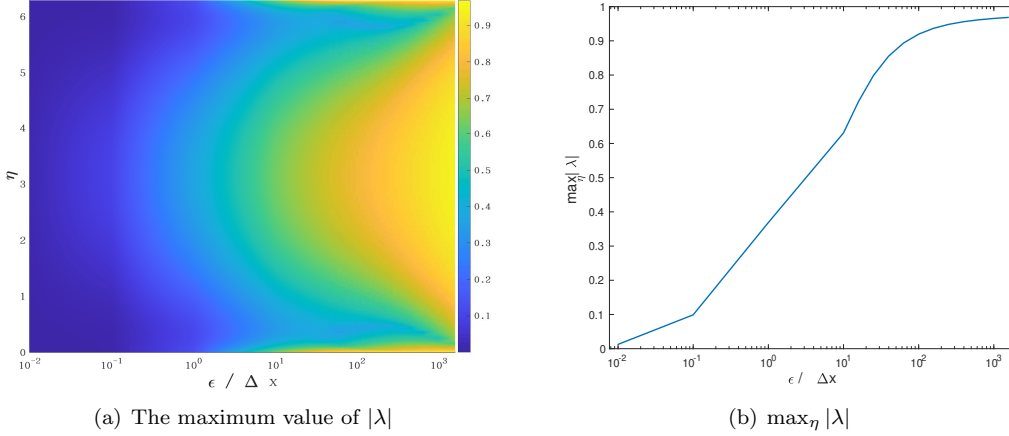


FIG. 1. The distribution of the maximum value of  $|\lambda|$ .

the two schemes, or more specifically, the equation  $\bar{\mathbf{u}}^{(n+1)} = \mathcal{T}_{\text{BSGS}}\bar{\mathbf{u}}^{(n)}$  refers to (3.3)(3.4), and  $\bar{\mathbf{u}}^{(n+1)} = \mathcal{T}_{\text{BSGS-MM}}\bar{\mathbf{u}}^{(n)}$  refers to (4.4)(4.5)(4.6). Then the Hybrid BSGS-MM method can be written as

$$\bar{\mathbf{u}}^{(n+1)} = \mathcal{T}_{\text{BSGS-MM}}(\mathcal{T}_{\text{BSGS}})^{N_b}\bar{\mathbf{u}}^{(n)}.$$

For large  $\epsilon$ , we tend to choose a larger  $N_b$  to gain better convergence. Note that when  $\epsilon$  is not spatially homogeneous, this scheme also allows to have different  $N_b$  for different spatial grids. We will study this method in our future works.

**4.3.2. The multiscale BSGS (BSGS-MS) method.** In equations (4.3), the moment equations are divided into two sets since  $\mathbf{u}^1$  and  $\mathbf{u}^2$  have different orders of magnitude with respect to  $\epsilon$ . This idea can be generalized if  $\mathbf{u}^2$  can be further separated to different magnitudes. Analysis on the magnitude of moments has been studied in several works including [29, 6, 31, 8]. These analyses may allow us to split  $\mathbf{u}$  into

$$(4.9) \quad \mathbf{u} = \begin{pmatrix} \mathbf{u}^1 \\ \mathbf{u}^2 \\ \vdots \\ \mathbf{u}^K \end{pmatrix},$$

so that  $\mathbf{u}^1, \dots, \mathbf{u}^K$  have increasing orders of magnitude with respect to  $\epsilon$ . Thus, the moment equations (2.4) can be rewritten in the following form:

$$\begin{cases} \mathbf{A}_{11} \frac{d\mathbf{u}^1}{dx} + \sum_{k=2}^K \mathbf{A}_{1k} \frac{d\mathbf{u}^k}{dx} = \frac{1}{\epsilon} \left( \mathbf{L}_{11}\mathbf{u}^1 + \sum_{k=2}^K \mathbf{L}_{1k}\mathbf{u}^k \right), \\ \mathbf{A}_{21} \frac{d\mathbf{u}^1}{dx} + \sum_{k=2}^K \mathbf{A}_{2k} \frac{d\mathbf{u}^k}{dx} = \frac{1}{\epsilon} \left( \mathbf{L}_{21}\mathbf{u}^1 + \sum_{k=2}^K \mathbf{L}_{2k}\mathbf{u}^k \right), \\ \dots, \\ \mathbf{A}_{K1} \frac{d\mathbf{u}^1}{dx} + \sum_{k=2}^K \mathbf{A}_{Kk} \frac{d\mathbf{u}^k}{dx} = \frac{1}{\epsilon} \left( \mathbf{L}_{K1}\mathbf{u}^1 + \sum_{k=2}^K \mathbf{L}_{Kk}\mathbf{u}^k \right), \end{cases}$$

where  $\mathbf{A}_{jk}$ ,  $j, k = 1, \dots, K$  are submatrices of  $\mathbf{A}$  determined by

$$\mathbf{A} = \begin{pmatrix} \mathbf{A}_{11} & \mathbf{A}_{21} & \cdots & \mathbf{A}_{K1} \\ \mathbf{A}_{12} & \mathbf{A}_{22} & \cdots & \mathbf{A}_{K2} \\ \vdots & \vdots & \ddots & \vdots \\ \mathbf{A}_{1K} & \mathbf{A}_{2K} & \cdots & \mathbf{A}_{KK} \end{pmatrix}.$$

Here  $\mathbf{u}^1$  can be chosen as the same vector as in (4.2) to guarantee the solvability of the first equation. The BSGS-MS method solves these equations one after another, so that the algorithm becomes

- (1) Set the error tolerance  $tol$  and the maximum number of iterations. Set  $n = 0$  and prepare the initial values  $\bar{\mathbf{u}}_j^{k,(0)}$  for  $j = 1, \dots, M$  and  $k = 1, \dots, K$  satisfying (3.2).
- (2) Solve  $\bar{\mathbf{u}}_j^{1,(n+1)}$  for all  $j = 1, 2, \dots, M$  by (4.4).
- (3) For  $k = 2, \dots, K$ , compute  $\bar{\mathbf{u}}_j^{k,(n+1)}$  by the following procedure:
  - (a) Calculate  $\bar{\mathbf{u}}_j^{k,(n+1/2)}$ ,  $j = 1, 2, \dots, M$  sequentially by

$$\begin{aligned} & -\mathbf{A}_{k1}^+ \bar{\mathbf{u}}_{j-1}^{1,(n+1)} + \left( |\mathbf{A}_{k1}| - \frac{1}{\epsilon} \Delta x \mathbf{L}_{k1} \right) \bar{\mathbf{u}}_j^{1,(n+1)} + \mathbf{A}_{k1}^- \bar{\mathbf{u}}_{j+1}^{1,(n+1)} \\ & = \sum_{l=2}^K \left[ \mathbf{A}_{kl}^+ \bar{\mathbf{u}}_{j-1}^{l,(n+1/2)} - \left( |\mathbf{A}_{kl}| - \frac{1}{\epsilon} \Delta x \mathbf{L}_{kl} \right) \bar{\mathbf{u}}_j^{l,(n+1/2)} - \mathbf{A}_{kl}^- \bar{\mathbf{u}}_{j+1}^{l,(n)} \right] \end{aligned}$$

where  $\bar{\mathbf{u}}_0^{:(\cdot)}$  and  $\bar{\mathbf{u}}_{M+1}^{:(\cdot)}$  are based on the boundary conditions.

- (b) Calculate  $\bar{\mathbf{u}}_j^{k,(n+1)}$ ,  $j = 1, 2, \dots, M$  in reverse order, that is to say,  $j = M, M-1, \dots, 2, 1$  by

$$\begin{aligned} & -\mathbf{A}_{k1}^+ \bar{\mathbf{u}}_{j-1}^{1,(n+1)} + \left( |\mathbf{A}_{k1}| - \frac{1}{\epsilon} \Delta x \mathbf{L}_{k1} \right) \bar{\mathbf{u}}_j^{1,(n+1)} + \mathbf{A}_{k1}^- \bar{\mathbf{u}}_{j+1}^{1,(n+1)} \\ & = \sum_{l=2}^K \left[ \mathbf{A}_{kl}^+ \bar{\mathbf{u}}_{j-1}^{l,(n+1/2)} - \left( |\mathbf{A}_{kl}| - \frac{1}{\epsilon} \Delta x \mathbf{L}_{kl} \right) \bar{\mathbf{u}}_j^{l,(n+1)} - \mathbf{A}_{kl}^- \bar{\mathbf{u}}_{j+1}^{l,(n+1)} \right] \end{aligned}$$

where  $\bar{\mathbf{u}}_0^{:(\cdot)}$  and  $\bar{\mathbf{u}}_{M+1}^{:(\cdot)}$  are based on the boundary conditions.

- (4) Compute the residual of the equations (3.1) for  $\bar{\mathbf{u}}_j = \bar{\mathbf{u}}_j^{(n+1)}$ ,  $j = 1, \dots, M$ . Stop if the norm of the residual is less than  $tol$ . Otherwise, check if  $n > N_s$ . If not, increase  $n$  by 1 and return to step (2). Otherwise, print warning messages about the failure of convergence and stop.

Again, when  $N$  is large, the number of components in  $\mathbf{u}^1$  is significantly less than  $N$ , leading to lower computational cost compared with the BSGS method. Another benefit of the BSGS-MS method is that the linear systems to be solved are smaller than both BSGS and BSGS-MM method.

**4.3.3. The Hybrid BSGS-MS method.** To obtain better convergence for large  $\epsilon$ , we can also combine the BSGS-MS method and the direct BSGS scans, leading to the ‘‘Hybrid BSGS-MS method’’. Such a method can be denoted by

$$\bar{\mathbf{u}}^{(n+1)} = \mathcal{T}_{\text{BSGS-MS}}(\mathcal{T}_{\text{BSGS}})^{N_b} \bar{\mathbf{u}}^{(n)},$$

where  $\mathcal{T}_{\text{BSGS-MS}}$  is the iteration operator for the BSGS-MS method.

**5. Numerical examples.** In this section, we are going to carry out some numerical tests to demonstrate the performances of BSGS and BSGS-MM methods for various Knudsen numbers  $\epsilon$ . For the first order finite volume methods (2.6) and (2.8), the following five methods will be tested:

- The BSGS method (section 3.1),
- The BSGS-MM method (section 4.1),
- The Hybrid BSGS-MM method with  $N_b$  BSGS steps per iteration, denoted as ‘‘Hybrid BSGS-MM- $N_b$ ’’ below (section 4.3.1),
- The BSGS-MS method (section 4.3.2)
- The Hybrid BSGS-MS method with  $N_b$  BSGS steps per iteration, denoted as ‘‘Hybrid BSGS-MS- $N_b$ ’’ below (section 4.3.3).

For the second-order schemes (2.7) and (2.9), we will also test the five methods mentioned above, with ‘‘BSGS’’ replaced with ‘‘BSSR’’, referring to a relaxation to improve the convergence (see 3.3). In all tests below, the relaxation parameter  $\alpha$  is chosen as  $1/4$ .

**5.1. One-dimensional tests: heat transfer.** We first consider a toy model in which both the spatial and velocity variables are one-dimensional. Below we will introduce the problem settings before showing our numerical results.



which are also applied to the boundary conditions (5.2). To uniquely determine the solution, the total mass needs to be specified:

$$\int_0^1 \rho(x) dx = 1, \quad \text{or} \quad \int_0^1 u^0(x) dx = 1.$$

In all our numerical tests, we choose  $T_w^0 = 0$  and  $T_w^1 = 1$ .

**5.1.2. Numerical results.** To verify the convergence of our method, we select  $N = 5$  for which the exact solution  $\mathbf{u}^{\text{exact}}(x)$  of (2.4) can be obtained analytically. The iteration is terminated if the residual has a norm less than  $10^{-10}$ . The density and temperature results for  $M = 40$  are given in Figure 2, from which one sees that both the first-order scheme (2.6) and the second-order scheme (2.7) provide results that are indistinguishable from the exact solution. We therefore test the order of convergence by checking the following  $L^2$  error of the solution:

$$\text{err} = \sqrt{\frac{1}{M} \sum_{j=1}^M \left\| \bar{\mathbf{u}}_j - \frac{1}{\Delta x} \int_{x_j - \Delta x/2}^{x_j + \Delta x/2} \mathbf{u}^{\text{exact}}(x) dx \right\|_2^2}.$$

The tests are carried out for  $\epsilon = 10^{-k}$  with  $k = 0, 1, 2, 3$  and  $M = 2^j \cdot 80$  with  $j = 0, 1, \dots, 5$ , and the errors of both schemes are displayed in Figure 3. It is clear that the desired order of convergence can be achieved in all cases, and the second-order scheme has a significantly lower numerical error. When  $\epsilon$  is smaller, the  $L^2$  error is larger, which is possibly due to the larger total variance in the exact solution as indicated in Figure 2.

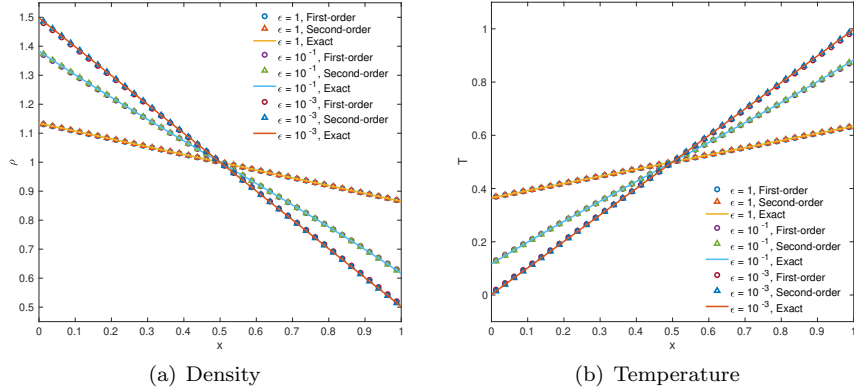


FIG. 2. The distributions of density and temperature with  $N = 5$ .

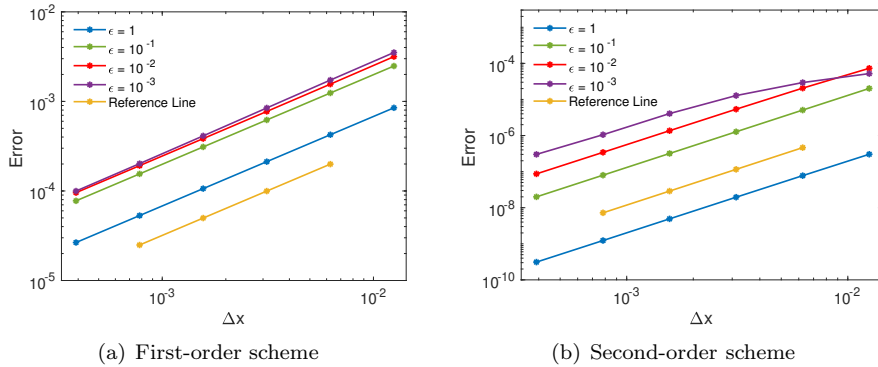


FIG. 3. The errors of upwind finite volume schemes for various  $\epsilon$ .

We now focus on the efficiency of different numerical methods. A larger moment system with  $N = 16$ , discretized on a uniform grid with  $\Delta x = 5 \times 10^{-3}$ , is considered in all the simulations below. The distributions of density  $\rho(x)$  and temperature  $T(x)$  calculated by second-order scheme (2.8) are performed in figure 4. We

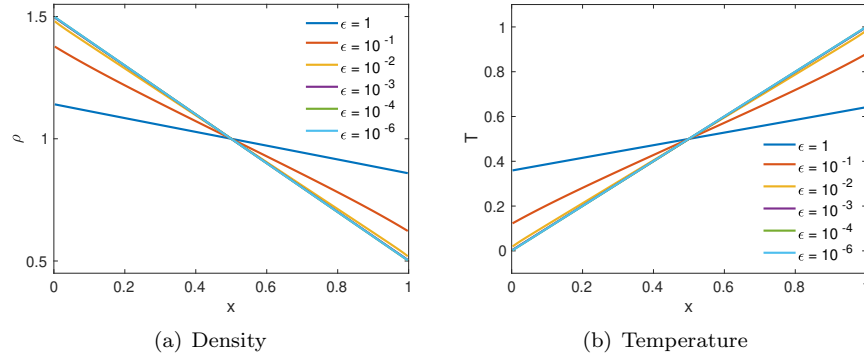


FIG. 4. The distributions of density and temperature with  $N = 16$ .

can see that the distributions of density and temperature almost coincide for  $\epsilon = 10^{-4}$  and  $10^{-6}$ . Totally, when  $\epsilon$  is less, they are closer and the values near the boundary are also closer to the boundary values, which means when  $\epsilon$  is small, there exists the boundary layer in the system. Also, the numerical results verifies the correctness of our algorithm.

Beginning with first-order method, we show in Figure 5 how the residual decreases in the BSGS method and the BSGS-MM methods where  $\mathbf{u}^1 = (u^0, u^1, u^2, u^3)$  in (4.2). For the BSGS method (Figures 5(a) and 5(b)), the trend of the curves agrees with the general behavior of the symmetric Gauss-Seidel method: the residual decreases quickly in the first few steps due to the fast elimination of high-frequency errors, and then the convergence slows down and the rate is governed by the lowest-frequency part of the error. More iterations are needed for smaller  $\epsilon$  as predicted in Theorem 3.2, but it can be expected that the convergence rate has a lower bound as stated in Theorem 3.1. On the contrary, the BSGS-MM method (Figure 5(c)) converges faster as  $\epsilon$  decreases, which is in line with our theoretical results in Section 4.2. When  $\epsilon \leq 10^{-4}$ , only one iteration is needed to meet our stopping criterion, since  $\mathbf{u}^2$  in (4.2) actually has magnitude  $O(\epsilon^2)$  and has little impact on the error of the solution.

Here we will take a closer look at the BSGS-MM method. Note that this approach requires solving the equation of  $\mathbf{u}^1$  (4.4) in every iteration. Despite the small number of components in  $\mathbf{u}^1$ , solving such a system, which is essentially the Navier-Stokes equations, could be nontrivial, especially in the multi-dimensional case. Although in the one-dimensional case, the equation can be solved efficiently by the Thomas algorithm, to better understand the computational cost in more general cases, we solve  $\mathbf{u}^1$  also by the BSGS iteration and the numbers of such inner iterations are given in Figure 6, where the horizontal axis denotes the outer iterations and the vertical axis denotes the number of inner iterations. In (4.9), we use  $\mathbf{u}^1 = (u^0, u^1, u^2, u^3)$  and  $\mathbf{u}^k = \mathbf{u}^{k-2}$ ,  $k = 2, \dots, N - 2$ . Note that the BSGS-MS method does not converge for  $\epsilon = 1, 10^{-1}$  and  $10^{-2}$ , and the BSGS-MM method also requires many outer iterations compared with other methods, which shows the importance of hybridizing with the BSGS method to bring down the high-frequency errors, and the figures show that the number of iterations is significantly reduced with  $N_b = 1$  only. In general, the number of inner iterations increases as  $\epsilon$  decreases. In the one-dimensional case, this indeed causes a rise of the computational cost, since  $\mathbf{u}^1$  occupies about a quarter of the total number of variables, which is non-negligible. Improvements can be made by adopting a better numerical solver for equations of  $\mathbf{u}^1$ , which is left to our future works.

Now we study second-order methods. We will first show that a direct application of the symmetric Gauss-Seidel method without relaxation may lead to divergent results. To this end, we apply the BSGS method and the BSSR method to the second-order scheme (2.9), and the results are given in Figure 7 for  $\epsilon = 1$  and  $10^{-4}$ . The BSGS method without relaxation quickly loses stability, and the BSSR method shows linear convergence for  $\epsilon = 1$ , but converges slowly for  $\epsilon = 10^{-4}$ , which is consistent with the first-order results. More results on the BSSR and BSSR-MM methods are plotted in Figure 8. Compared with Figure 5, the general behaviors of both methods are similar, but the iterative methods for second-order methods

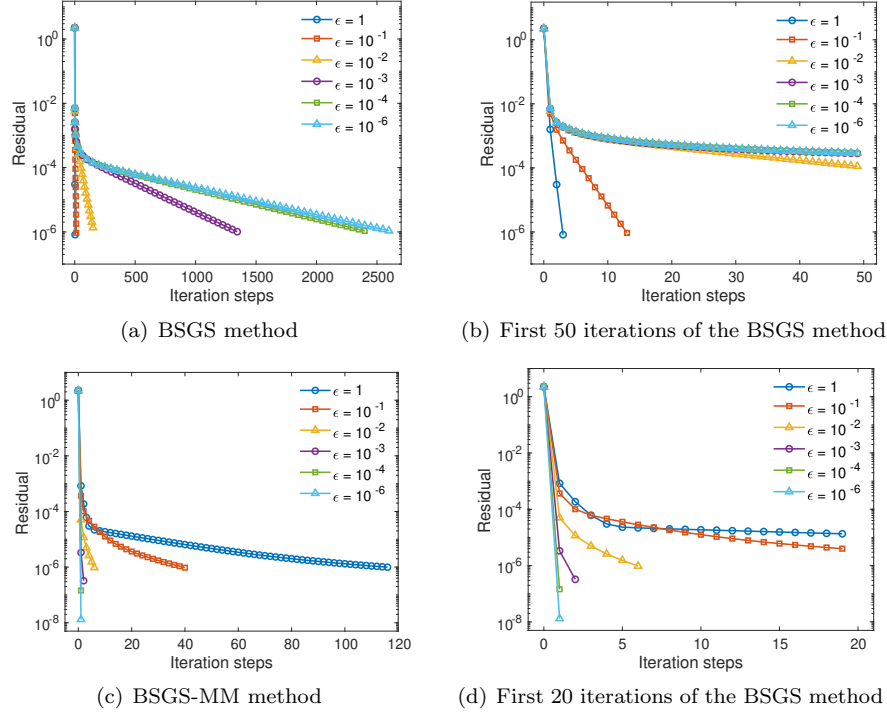


FIG. 5. The convergence rate of BSGS and BSGS-MM methods for the one-dimensional heat transfer.

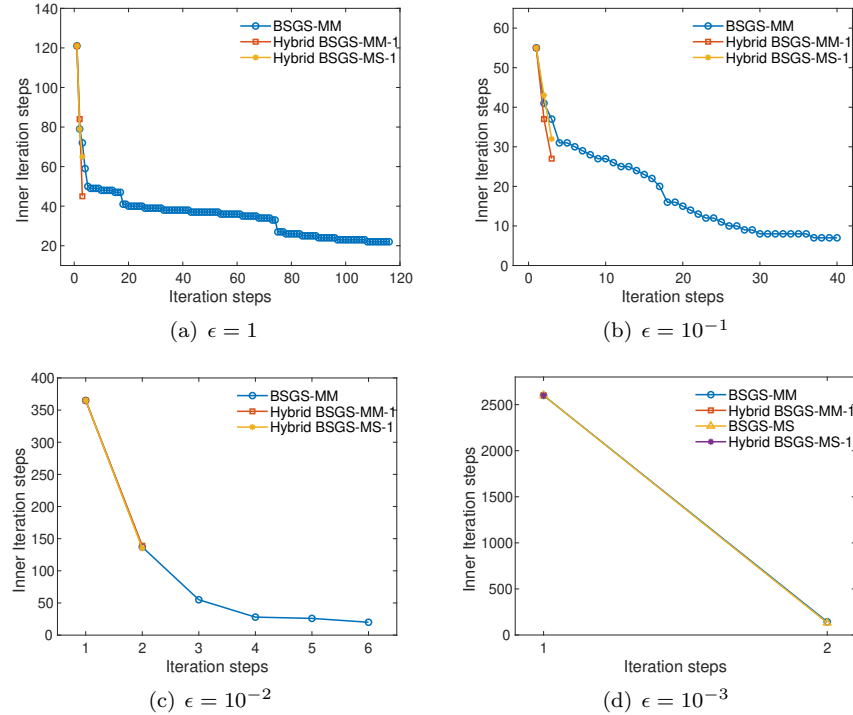


FIG. 6. The inner iterations of (Hybrid) BSGS-MM and BSGS-MS methods for the one-dimensional heat transfer.

converge more slowly for the same grid size due to the more complicated structures of the matrices. The numbers of inner iterations to solve  $u^1$  for various methods are displayed in Figure 9. One can again see that inside each outer iteration, more inner iterations are needed for smaller  $\epsilon$ . The BSSR-MS method again

diverges for  $\epsilon = 1$ ,  $10^{-1}$  and  $10^{-2}$ , and even the Hybrid BSSR-MS-1 method does not converge for in these three cases. We therefore increase the value of  $N_b$  in our experiments. For larger  $\epsilon$ , a larger value of  $N_b$  is needed, and the number of inner iterations can also be found in Figure 9.

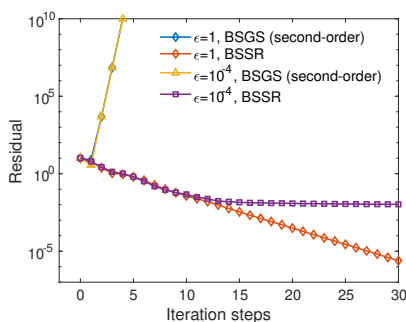


FIG. 7. The convergence of BSGS and BSSR method for the second-order scheme.

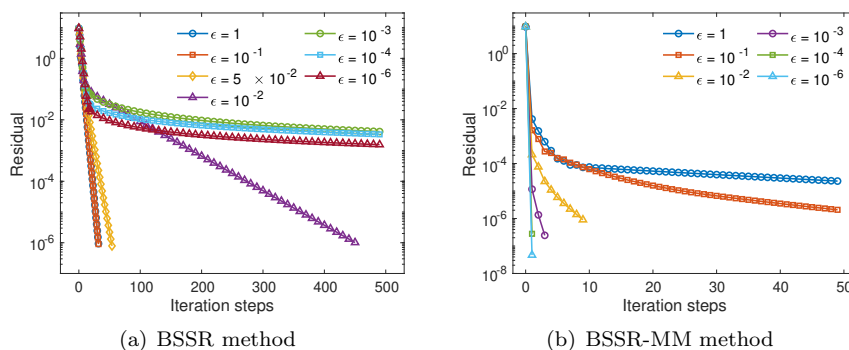


FIG. 8. The convergence of the BSSR and BSSR-MM methods for the one-dimensional heat transfer.

Lastly, we compare the actual computational time for all the above methods. The data are listed in Table 1. For large  $\epsilon$ , the BSGS (or BSSR) method always has the best performance. When  $\epsilon$  gets smaller, the performance of other methods is improved. In particular, the Hybrid BSSR-MM method and the Hybrid BSSR-MS method have similar computational times. However, in this one-dimensional toy model, the number of components in  $\mathbf{u}^1$  is still about 1/4 of the total number of variables, and solving the equation of  $\mathbf{u}^1$  takes a large amount of time when  $\epsilon$  is small. As a result, the BSGS and the BSSR methods still hold the best performance for  $\epsilon = 10^{-6}$ , even if other methods require only one iteration. In the next section, we will consider the three-dimensional velocity space, so that the proportion of  $\mathbf{u}^1$  in  $\mathbf{u}$  will become smaller.

TABLE 1  
Computing time for the one-dimensional heat transfer (measure time by the second).

		$\epsilon = 1$	$\epsilon = 10^{-1}$	$\epsilon = 10^{-2}$	$\epsilon = 10^{-3}$	$\epsilon = 10^{-4}$	$\epsilon = 10^{-6}$
First order	BSGS	0.0042	0.0383	0.1182	0.7626	1.2799	1.4125
	BSGS-MM	2.2980	0.6766	0.3534	1.1341	1.7307	1.8482
	Hybrid BSGS-MM-1	0.1275	0.1746	0.4342	1.0431	1.7575	1.9325
	BSGS-MS	—	—	—	1.0499	1.7966	1.9426
	Hybrid BSGS-MS-1	0.1447	0.1796	0.4480	1.0000	1.8690	1.8713
Second order	BSSR	0.0585	0.1302	0.6447	10.220	88.469	2350.6
	BSSR-MM	9.2520	1.7299	1.2873	9.5040	66.147	4103.9
	Hybrid BSSR-MM-1	1.2217	0.5678	1.4010	9.2619	68.572	4277.2
	BSSR-MS	—	—	—	9.3642	69.734	4276.2
	Hybrid BSSR-MS- $N_b$	1.3608	0.6585	1.6115	9.8017	66.349	4265.6
		$(N_b = 6)$	$(N_b = 4)$	$(N_b = 3)$	$(N_b = 1)$	$(N_b = 1)$	$(N_b = 1)$

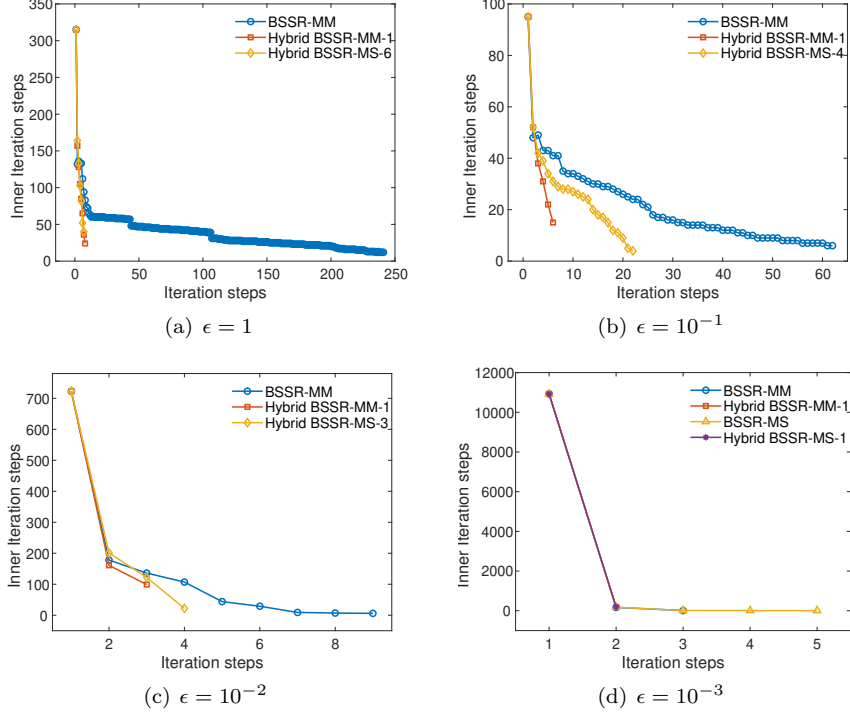


FIG. 9. The inner iterations of (Hybrid) BSSR-MM and BSSR-MS methods for the one-dimensional heat transfer.

**5.2. Examples with two-dimensional space and three-dimensional velocity.** To reflect a more realistic case, we study the following linearized Boltzmann equation with  $\mathbf{x} \in \mathbb{R}^2$  and  $\mathbf{v} \in \mathbb{R}^3$ :

$$v_1 \frac{\partial}{\partial x_1} f(\mathbf{x}, \mathbf{v}) + v_2 \frac{\partial}{\partial x_2} f(\mathbf{x}, \mathbf{v}) = \frac{1}{\epsilon} \mathcal{L}[f](\mathbf{x}, \mathbf{v}),$$

and we adopt the expansion of the distribution function in [18, 15] using Burnett polynomials:

$$(5.3) \quad f(\mathbf{x}, \mathbf{v}) = \sum_{l=0}^{\infty} \sum_{m=-l}^l \sum_{n=0}^{\infty} u^{lmn}(\mathbf{x}) \varphi_{lmn}(\mathbf{v}) \omega(\mathbf{v}).$$

The polynomials  $\varphi_{lmn}$  are defined by

$$\varphi_{lmn}(\mathbf{v}) = |\mathbf{v}|^l Y_{lm} \left( \frac{\mathbf{v}}{|\mathbf{v}|} \right) L_n^{(l+1/2)} \left( \frac{|\mathbf{v}|^2}{2} \right)$$

where  $Y_{lm}(\cdot)$  are real spherical harmonics [5]. The weight function is again an isotropic Gaussian centered at the origin:

$$\omega(\mathbf{v}) = \frac{1}{(\sqrt{2\pi})^3} \exp \left( -\frac{|\mathbf{v}|^2}{2} \right).$$

The collision operator  $\mathcal{L}$  is chosen based on Maxwell molecules, so that the matrix  $\mathbf{L}$  in (3.5) is diagonal. Some of the diagonal values are given by the following facts:

$$\begin{aligned} \mathcal{L}[\varphi_{000}\omega] &= 0, & \mathcal{L}[\varphi_{001}\omega] &= 0, & \mathcal{L}[\varphi_{100}\omega] &= 0, & \mathcal{L}[\varphi_{1m1}\omega] &= -\frac{2}{3}\varphi_{1m1}\omega, & \mathcal{L}[\varphi_{2m0}\omega] &= -\varphi_{2m0}\omega, \\ \mathcal{L}[\varphi_{002}\omega] &= -\frac{2}{3}\varphi_{002}\omega, & \mathcal{L}[\varphi_{1m2}\omega] &= -\varphi_{1m2}\omega, & \mathcal{L}[\varphi_{2m1}\omega] &= -\frac{7}{6}\varphi_{2m1}\omega, & \mathcal{L}[\varphi_{3m0}\omega] &= -\frac{3}{2}\varphi_{3m0}\omega. \end{aligned}$$

More coefficients can be found in [2]. The macroscopic quantities including the density, velocity and the temperature are related to the coefficients by

$$\begin{aligned} \rho(\mathbf{x}) &= \frac{1}{2\sqrt{\pi}}u_{000}(\mathbf{x}), & T(\mathbf{x}) &= -\frac{1}{2\sqrt{\pi}}u_{001}(\mathbf{x}), \\ U_1(\mathbf{x}) &= \frac{1}{2}\sqrt{\frac{3}{\pi}}u_{110}(\mathbf{x}), & U_2(\mathbf{x}) &= \frac{1}{2}\sqrt{\frac{3}{\pi}}u_{1,-1,0}(\mathbf{x}), & U_3(\mathbf{x}) &= \frac{1}{2}\sqrt{\frac{3}{\pi}}u_{100}(\mathbf{x}). \end{aligned}$$

The truncation of the infinite series (5.3) is done by selecting a positive integer  $L$ , and then reserve terms with  $l = 0, 1, \dots, L$  and  $m = -l, \dots, l$ ,  $n = 0, 1, \dots, \lceil(L-l)/2\rceil$ . The solution  $\mathbf{u}$  is then a vector composed of  $u^{lmn}$  with  $l, m, n$  within the above range, and the two-dimensional moment equations can be formulated as

$$(5.4) \quad \mathbf{A}_1 \frac{\partial \mathbf{u}}{\partial x_1} + \mathbf{A}_2 \frac{\partial \mathbf{u}}{\partial x_2} = \frac{1}{\epsilon} \mathbf{L} \mathbf{u}.$$

Such a choice of the truncation covers the classical Euler equations ( $L = 1$ ), Grad's 13-moment equations ( $L = 2$ ) and Grad's 26-moment equations ( $L = 3$ ). In the following sections, two test cases will be studied under these settings.

**5.2.1. Heat transfer in a cavity.** The first test case is a heat transfer problem where the domain is a unit square  $\Omega = (0, 1) \times (0, 1)$ . The boundaries can have different temperatures, causing heat transfer inside the chamber. All walls are fully diffusive, so that the boundary conditions of the moment equations (5.4) can again be formulated according to Appendix A. In our test, we set the temperature of the top wall  $(0, 1) \times \{1\}$  to be 1, and all other walls have temperature 0. Numerically, the boundary conditions are processed using the ghost-cell method as in the one-dimensional case (5.2). To uniquely determine the solution, we again set the total mass to be 1:

$$\int_{\Omega} \rho(\mathbf{x}) \, d\mathbf{x} = \frac{1}{2\sqrt{\pi}} \int_{\Omega} u^{000}(\mathbf{x}) \, d\mathbf{x} = 1.$$

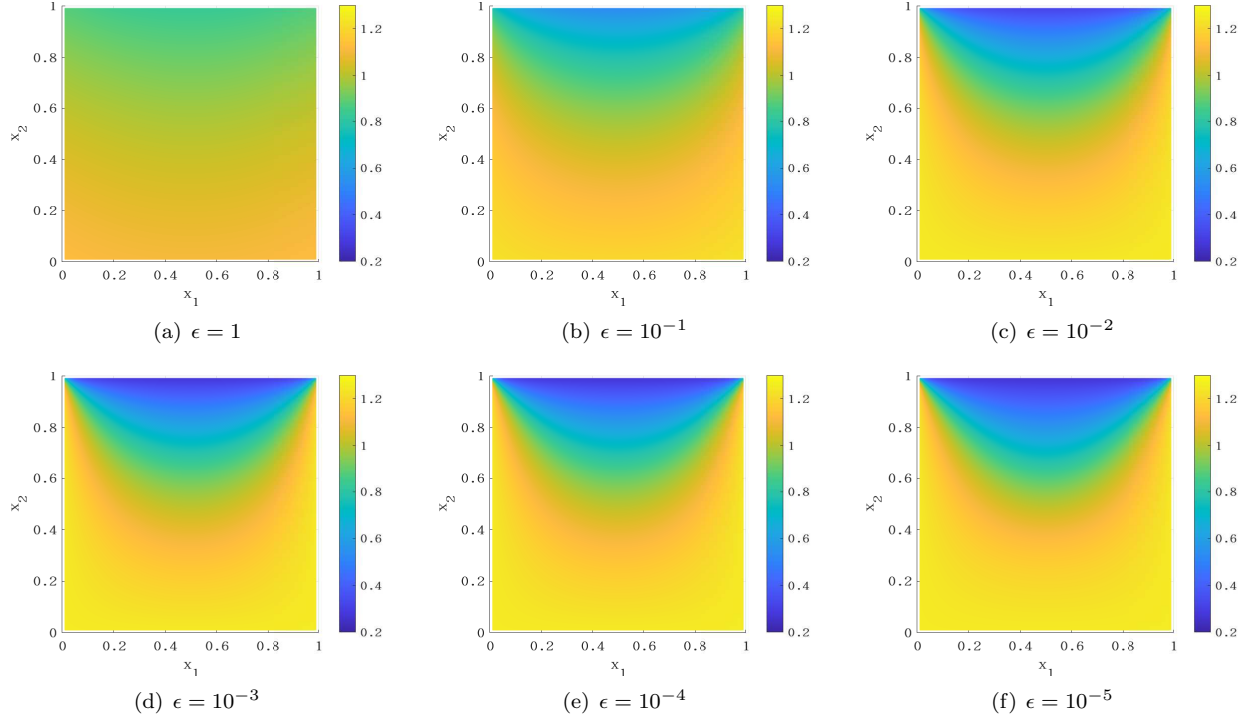
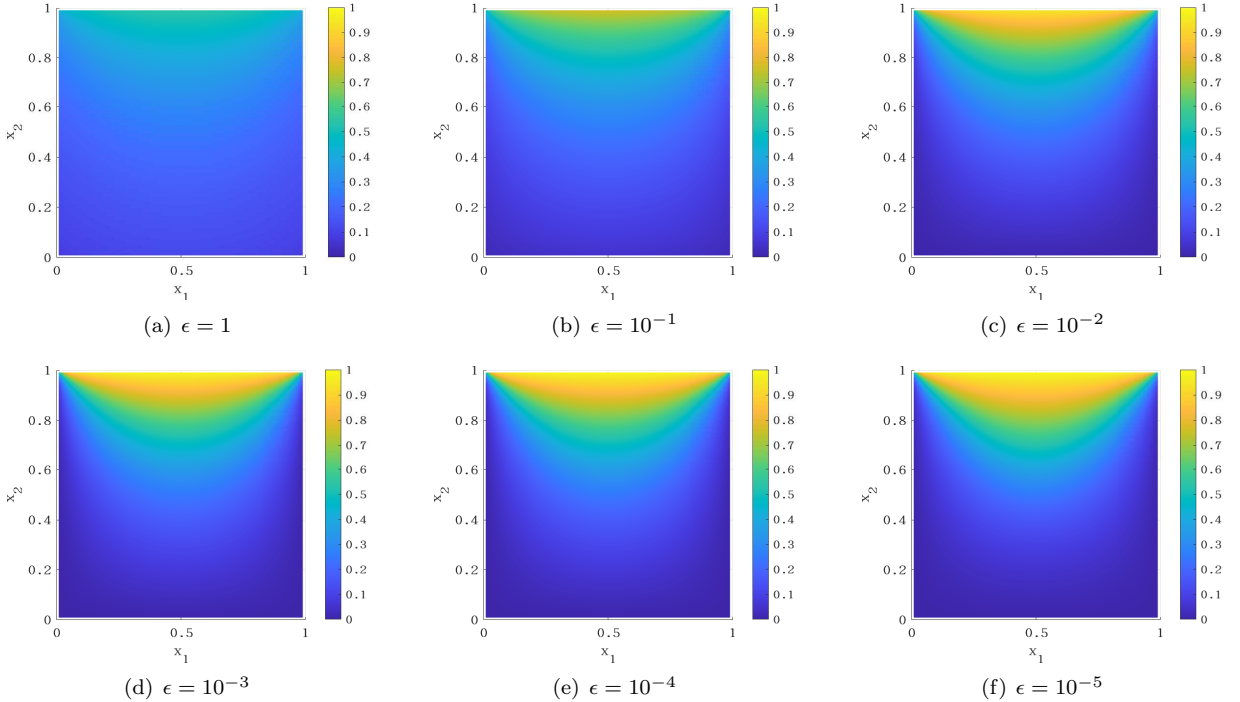
To solve the heat transfer problem, we use a  $50 \times 50$  uniform grid to discretize the spatial domain, and choose  $L = 10$  in the truncation of the series (5.3). The total number of equations is 341. The macroscopic part of the solution  $\mathbf{u}^1$  in (4.2) and (4.9) consists of 13 variables, including all  $u^{lmn}$  with  $l \leq 2$  and  $n \leq \lceil(2-l)/2\rceil$ . Thus, the equations of  $\mathbf{u}^1$  are essentially Grad's 13-moment equations, which are equivalent to the Navier-Stokes equations in the linear, steady-state case. In (4.9), by asymptotic analysis [29], the vector  $\mathbf{u}^k$  for  $k = 2, \dots, L-1$  is chosen as a vector consisting of all variables in  $\mathcal{U}_{k+1} \setminus \mathcal{U}_k$  with

$$\mathcal{U}_k = \{u^{lmn} \mid l = 0, 1, \dots, k, \quad m = -l, \dots, l, \quad n = 0, \dots, \lceil(k-l)/2\rceil\}.$$

The numerical solutions of the density and temperature computed using the second-order method are displayed in Figures 10 and 11. For larger  $\epsilon$ , both the density and temperature in the domain distribute more homogeneously, and the temperature jump on the top wall becomes more obvious, leading to a large discontinuity in the top-left and top-right corners.

We first study the performance of the iterative methods applied to the first-order scheme (2.8). The norm of the residual versus the number of iterations is given in Figure 12 for the BSGS and BSGS-MM methods. In this test case, even for  $\epsilon = 0.1$ , the BSGS-MM method reaches the threshold  $10^{-6}$  within 20 iterations, which is faster than the BSGS method. However, it fails to converge for  $\epsilon = 1$ . Interestingly, the Hybrid BSGS-MM method does not converge for  $\epsilon = 1$  as well, even if we increase  $N_b$  to 20. Further increasing  $N_b$  is meaningless since the BSGS method requires only 47 steps to reach the threshold of the residual. The Hybrid BSGS-MM method converges when  $N_b$  is set to be 6, and the number of inner iteration for solving the equations of  $\mathbf{u}^1$  is given in Figure 13(a). Figure 13 also gives results for other values of  $\epsilon$ . When  $\epsilon = 10^{-1}$ , the BSGS-MM method still fails to converge, but all other methods perform quite well. In general, when  $\epsilon$  decreases, more inner iteration steps are required to solve the 13-moment equations, but this part takes a relatively small proportion of the total computational cost due to its small number of variables.

The behavior of iterative methods for the second-order method (2.9) is generally the same, but Figure 14 shows that the BSSR method requires more iterations to converge compared with the first-order method, and the BSSR-MM method diverges even for  $\epsilon = 10^{-1}$ . The numbers of inner iterations are given in Figure

FIG. 10. *The distributions of density for the heat transfer in a cavity.*FIG. 11. *The distributions of temperature for the heat transfer in a cavity.*

15, but we again emphasize that such data become less significant when  $\mathbf{u}^1$  only takes up a small proportion of the entire solution. It is worth mentioning that when  $\epsilon = 1$ , the Hybrid BSSR-MM also fails to converge for a reasonable choice of  $N_b$ .

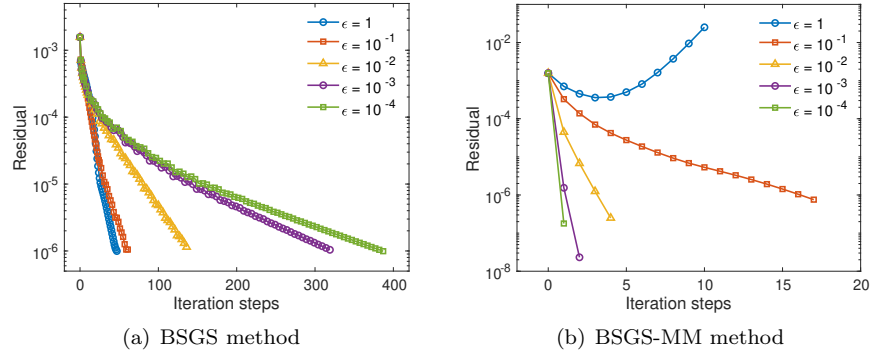


FIG. 12. The convergence rate of BSGS and BSGS-MM methods for the heat transfer in a cavity.

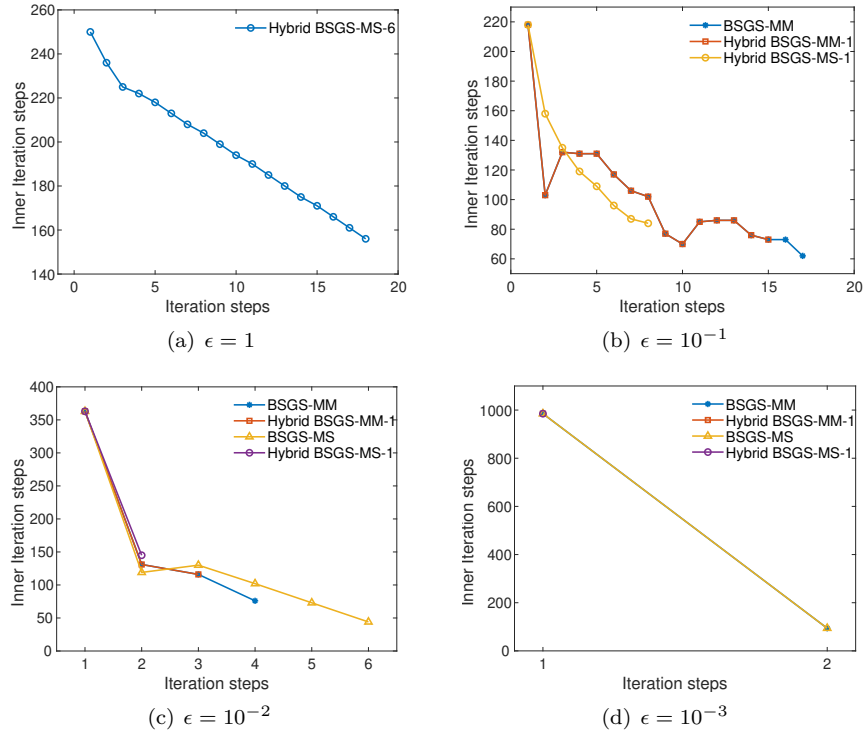


FIG. 13. The inner iterations of (Hybrid) BSGS-MM and BSGS-MS methods for the heat transfer in a cavity.

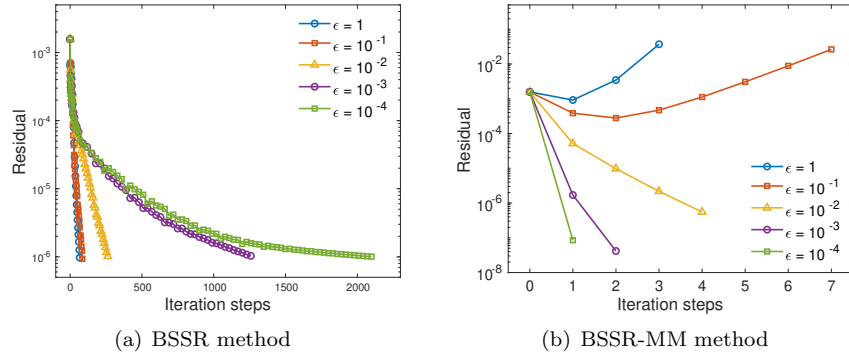


FIG. 14. The convergence rate of BSSR and BSSR-MM methods for the heat transfer in a cavity.

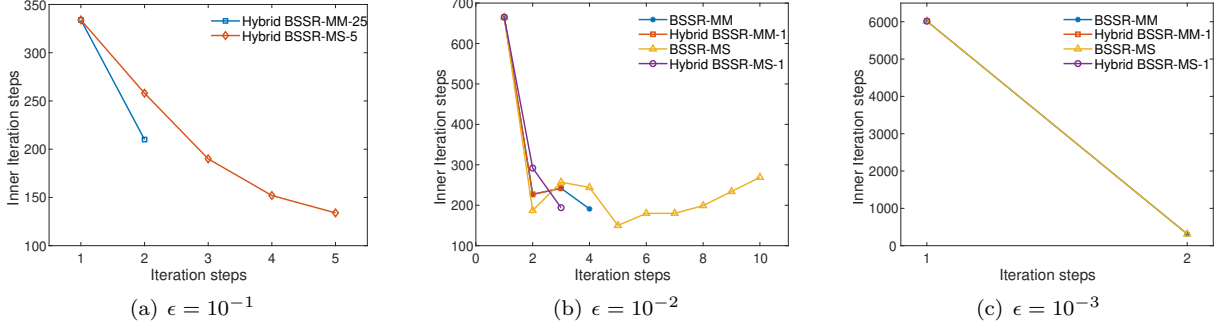


FIG. 15. The inner iterations of (Hybrid) BSSR-MM and BSSR-MS methods for the heat transfer in a cavity.

To summarize, we tabulate the computational time of all the methods above in Table 2. It is clear that for large  $\epsilon$ , the BSGS/BSSR method is still the optimal choice among this family of approaches. On the other end, when  $\epsilon = 10^{-4}$ , all methods with the micro-macro or multiscale decomposition have similar performances since they have only one or two outer iterations. Averagely, the Hybrid BSGS-MS/BSSR-MS method has the best performance since it only requires solving small matrices in each iteration. In these tests, when  $\epsilon$  is close to zero, the computational cost is still high due to the inefficiency of solving the 13-moment equations (or Navier-Stokes-Fourier equations). This can be improved by adopting a better solver for the equations of  $\mathbf{u}^1$ .

TABLE 2  
Computing time for the heat transfer in a cavity (measure time by the second).

		$\epsilon = 1$	$\epsilon = 10^{-1}$	$\epsilon = 10^{-2}$	$\epsilon = 10^{-3}$	$\epsilon = 10^{-4}$	
First order	BSGS	140.17	183.84	410.29	950.68	1127.8	
	BSGS-MM	–	93.790	40.277	65.446	71.606	
	Hybrid BSGS-MM-1	–	102.51	43.035	55.705	70.045	
	BSGS-MS	–	–	42.597	59.723	69.711	
	Hybrid BSGS-MS- $N_b$	321.56	57.126	22.851	32.920	70.575	
		$(N_b = 6)$	$(N_b = 1)$	$(N_b = 1)$	$(N_b = 1)$	$(N_b = 1)$	
Second order	BSSR	678.13	881.67	2714.7	13139	21693	
	BSSR-MM	–	–	124.23	348.22	2530.4	
	Hybrid BSSR-MM- $N_b$	–	391.28	124.66	341.44	2579.6	
				$(N_b = 25)$	$(N_b = 1)$	$(N_b = 1)$	$(N_b = 1)$
	BSSR-MS	–	–	125.03	351.18	2513.2	
Hybrid BSSR-MS- $N_b$	–	258.07	125.83	342.41	2558.9		
			$(N_b = 5)$	$(N_b = 1)$	$(N_b = 1)$	$(N_b = 1)$	

**5.2.2. Cavity flow.** Lid-driven cavity flow is another common benchmark test for two-dimensional rarefied flows. We again assume that the gas is confined in a square cavity  $\Omega = (0, 1) \times (0, 1)$ . All the walls have the same temperature. The top lid at  $y = 1$  has a horizontal velocity  $\mathbf{U}_w = (1, 0)^T$ , and all other walls are stationary. The boundary conditions of moment methods can again be formulated according to Appendix A. In our tests, we again choose  $L = 10$  and the grid size to be  $50 \times 50$ . Only the second-order scheme (2.9) is tested in our experiments. The numerical results for the temperature and the streamlines of the heat flux are plotted in Figure 16. Note that the heat flux  $\mathbf{q}$  can also be obtained directly from the variables  $u^{lmn}$  by

$$q_1(\mathbf{x}) = -\frac{5}{4}\sqrt{\frac{3}{\pi}}u_{111}(\mathbf{x}), \quad q_2(\mathbf{x}) = -\frac{5}{4}\sqrt{\frac{3}{\pi}}u_{1,-1,1}(\mathbf{x}), \quad q_3(\mathbf{x}) = -\frac{5}{4}\sqrt{\frac{3}{\pi}}u_{101}(\mathbf{x}).$$

For large Knudsen numbers, it can be observed in the plots that the heat transfers from the cold area to the hot area, which is one of the typical rarefaction effects.

Table 3 lists the computational time of all the five iterative methods. The Hybrid BSSR-MS method again shows its competitiveness in most cases, despite its divergence for  $\epsilon = 1$ . For  $\epsilon = 10^{-3}$  and  $10^{-4}$ ,

all methods except BSSR requires only one outer iteration, and again the performance is limited by the Navier-Stokes solver, which is to be improved in our future works.

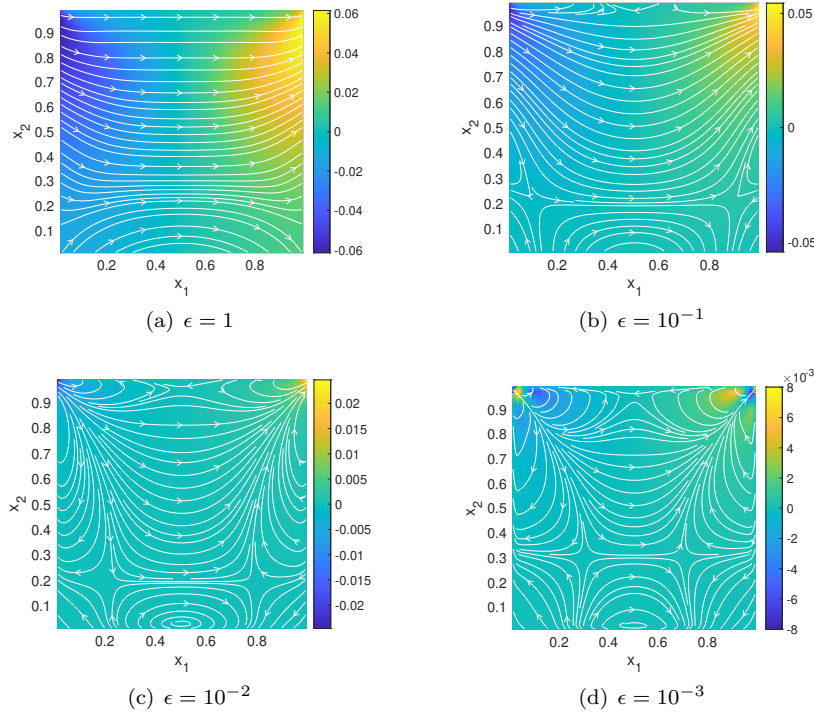


FIG. 16. The distributions of temperature and the streamline of heat flux for the lid-driven cavity flow.

TABLE 3  
Computing time for the lid-driven cavity flow (measure time by the second).

		$\epsilon = 1$	$\epsilon = 10^{-1}$	$\epsilon = 10^{-2}$	$\epsilon = 10^{-3}$	$\epsilon = 10^{-4}$
Second order	BSSR	836.52	1031.3	2908.0	11322	21591
	BSSR-MM	–	–	132.47	297.18	1354.6
	Hybrid BSSR-MM-1	–	–	141.85	281.39	1349.2
	BSSR-MS	–	–	–	294.17	1370.5
	Hybrid BSSR-MS- $N_b$	–	306.53 ( $N_b = 5$ )	129.35 ( $N_b = 1$ )	284.82 ( $N_b = 1$ )	1356.3 ( $N_b = 1$ )

**6. Conclusion.** We have studied a family of iterative methods for solving steady-state linearized moment equations. Generally speaking, the BSGS method works well for highly rarefied gases, but the convergence slows down as the Knudsen number decreases. On the contrary, the BSGS-MM method has better efficiency in the dense regime. Better performance can be achieved by coupling these two methods. Our numerical tests confirm the theoretical analysis of our methods. However, the experiments also reveal some practical issues:

- Although the Fourier analysis confirms the convergence of both BSGS and BSGS-MM methods for a wide range of  $\epsilon$ , when the wall boundary conditions are imposed, the BSGS-MM method may still diverge for large  $\epsilon$ , especially when the method is generalized to second-order schemes. This requires more careful analysis of the iterative method on bounded domains, which is a part of our ongoing work.
- In methods with micro-macro or multiscale decomposition, the inner iteration may take a significant amount of time despite a very small number of outer iterations. Usually the macroscopic part is essentially Euler or Navier-Stokes equations. One can replace the simple BSGS solver used in this

work with more specific solvers to gain improved efficiency.

The general idea of this family of approaches is also applicable to nonlinear moment methods. The moment method has been applied to the time-dependent Boltzmann equation with the quadratic collision term in [15], and the combination of the symmetric Gauss-Seidel method and the multigrid technique has been tested for steady-state moment equations of BGK-type collisions, where the ansatz for the distribution function is nonlinear [16]. In our future work, we will try to integrate the micro-macro/multiscale decomposition to these nonlinear equations to enhance the performance of the iterative methods.

### Appendix A. Boundary conditions of moment equations.

Given a unit vector  $\mathbf{n}$ , we say  $u^n$  in (2.2) is an *odd moment* if the corresponding basis function  $\varphi_n$  satisfies

$$\varphi_n(\mathbf{v} - 2(\mathbf{v} \cdot \mathbf{n})\mathbf{n}) = -\varphi_n(\mathbf{v}), \quad \forall \mathbf{v} \in \mathbb{R}^d.$$

Similarly, a moment  $u^n$  is said to be an *even moment* if

$$\varphi_n(\mathbf{v} - 2(\mathbf{v} \cdot \mathbf{n})\mathbf{n}) = \varphi_n(\mathbf{v}), \quad \forall \mathbf{v} \in \mathbb{R}^d.$$

In our test cases, all moments are either odd or even if  $\mathbf{n}$  is a normal unit vector on the boundary. According to [13], the boundary conditions should be imposed only on odd moments. For a given moment system for  $\mathbf{u} = (u^0, u^1, \dots, u^N)^T$ , we define  $\mathcal{I}_{\text{odd}}$  to be the index set such that  $u^n$  is an odd moment if  $n \in \mathcal{I}_{\text{odd}}$ , and let  $\mathcal{I}_{\text{even}} = \{0, 1, \dots, N\} \setminus \mathcal{I}_{\text{odd}}$ . In  $\mathcal{I}_{\text{odd}}$ , there is a special index  $k$  such that the moment  $u^k$  is proportional to the normal velocity. Assume that the boundary can have a tangential velocity  $\mathbf{U}_w$  satisfying  $\mathbf{U}_w \cdot \mathbf{n} = 0$ . According to [26], the fully diffusive wall boundary conditions should hold the following form:

$$\begin{aligned} u^k &= 0, \\ u^n &= -2 \sum_{n_1 \in \mathcal{I}_{\text{odd}} \setminus \{k\}} \sum_{n_2 \in \mathcal{I}_{\text{even}}} \left( Q_{nn_1} - \frac{Q_{nk} Q_{kn_1}}{Q_{kk}} \right) A_{n_1 n_2} (u^{n_2} - \mathbf{U}_w \cdot \mathcal{M}_U^{n_2} - T_w \mathcal{M}_T^{n_2}), \quad n \in \mathcal{I}_{\text{odd}} \setminus \{k\}, \end{aligned}$$

where  $\mathbf{U}_w$  and  $T_w$  refers to the wall velocity and temperature, respectively, and

$$\begin{aligned} Q_{nn_1} &= \frac{\int_{\mathbb{R}^d} (\mathbf{v} \cdot \mathbf{n})^{-1} \varphi_n(\mathbf{v}) \varphi_{n_1}(\mathbf{v}) \omega(\mathbf{v}) \, d\mathbf{v}}{\int_{\mathbb{R}^d} |\varphi_n(\mathbf{v})|^2 \omega(\mathbf{v}) \, d\mathbf{v}}, & A_{n_1 n_2} &= \frac{\int_{\mathbb{R}^d} (\mathbf{v} \cdot \mathbf{n}) \varphi_{n_1}(\mathbf{v}) \varphi_{n_2}(\mathbf{v}) \omega(\mathbf{v}) \, d\mathbf{v}}{\int_{\mathbb{R}^d} |\varphi_{n_1}(\mathbf{v})|^2 \omega(\mathbf{v}) \, d\mathbf{v}}, \\ \mathcal{M}_U^{n_2} &= \frac{\int_{\mathbb{R}^d} \mathbf{v} \varphi_{n_2}(\mathbf{v}) \omega(\mathbf{v}) \, d\mathbf{v}}{\int_{\mathbb{R}^d} |\varphi_{n_2}(\mathbf{v})|^2 \omega(\mathbf{v}) \, d\mathbf{v}}, & \mathcal{M}_T^{n_2} &= \frac{\int_{\mathbb{R}^d} (|\mathbf{v}|^2 - d) \varphi_{n_2}(\mathbf{v}) \omega(\mathbf{v}) \, d\mathbf{v}}{2 \int_{\mathbb{R}^d} |\varphi_{n_2}(\mathbf{v})|^2 \omega(\mathbf{v}) \, d\mathbf{v}}. \end{aligned}$$

These boundary conditions can be written in the matrix form as

$$\mathbf{u}^{\text{odd}} = \mathbf{B} \mathbf{u}^{\text{even}} - T_w \mathbf{g}.$$

### REFERENCES

- [1] M. ADAMS AND E. LARSEN, *Fast iterative methods for discrete-ordinates particle transport calculations*, Progress in Nuclear Energy, 40 (2002), pp. 3–159.
- [2] Z. ALTERMAN, K. FRANKOWSKI, AND C. L. PEKERIS, *Eigenvalues and eigenfunctions of the linearized Boltzmann collision operator for a Maxwell gas and for a gas of rigid spheres*, The Astrophysical Journal Supplement series, 7 (1962), pp. 291–331.
- [3] J. BALITI, M. HSSIKOU, AND M. ALAOU, *The 13-moments method for heat transfer in gas microflows*, Australian J. Mech. Eng., 18 (2020), pp. 80–93.
- [4] M. BENNOUNE, M. LEMOU, AND L. MIEUSSENS, *Uniformly stable numerical schemes for the Boltzmann equation preserving the compressible Navier-Stokes asymptotics*, J. Comput. Phys., 227 (2008), pp. 3781–3803.
- [5] M. A. BLANCO, M. FLÓREZ, AND M. BERMEJO, *Evaluation of the rotation matrices in the basis of real spherical harmonics*, Journal of Molecular structure: THEOCHEM, 419 (1997), pp. 19–27.
- [6] Z. CAI, R. LI, AND Y. WANG, *Numerical regularized moment method for high mach number flow*, Comm. Comput. Phys., 11 (2012), pp. 1415–1438.
- [7] Z. CAI AND M. TORRILHON, *On the Holway-Weiss debate: Convergence of the Grad-moment-expansion in kinetic gas theory*, Phys. Fluids, 31 (2020), p. 126105.
- [8] Z. CAI, M. TORRILHON, AND S. YANG, *Linear regularized 13-moment equations with Onsager boundary conditions for general gas molecules*, 2023. To appear in SIAM J. Appl. Math.
- [9] C. CERCIGNANI AND C. CERCIGNANI, *The boltzmann equation*, Springer, 1988.

- [10] T. F. CHAN AND H. C. ELMAN, *Fourier analysis of iterative methods for elliptic pr*, SIAM review, 31 (1989), pp. 20–49.
- [11] S. CHAPMAN AND T. G. COWLING, *The mathematical theory of non-uniform gases: an account of the kinetic theory of viscosity, thermal conduction and diffusion in gases*, Cambridge university press, 1990.
- [12] G. DIMARCO, R. LOUBÉRE, J. NARSKI, AND T. REY, *An efficient numerical method for solving the Boltzmann equation in multidimensions*, J. Comput. Phys., 353 (2018), pp. 46–81.
- [13] H. GRAD, *On the kinetic theory of rarefied gases*, Communications on pure and applied mathematics, 2 (1949), pp. 331–407.
- [14] X. GU AND D. R. EMERSON, *A high-order moment approach for capturing non-equilibrium phenomena in the transition regime*, J. Fluid Mech., 636 (2009), pp. 177–216.
- [15] Z. HU AND Z. CAI, *Burnett spectral method for high-speed rarefied gas flows*, SIAM J. Sci. Comput., 42 (2020), pp. B1193–B1226.
- [16] Z. HU AND G. HU, *An efficient steady-state solver for microflows with high-order moment model*, J. Comput. Phys., 392 (2019), pp. 462–482.
- [17] S. JAISWAL, A. A. ALEXEENKO, AND J. HU, *A discontinuous Galerkin fast spectral method for the full Boltzmann equation with general collision kernels*, J. Comput. Phys., 378 (2019), pp. 178–208.
- [18] K. KUMAR, *Polynomial expansions in kinetic theory of gases*, Ann. Phys., 37 (1966), pp. 113–141.
- [19] R. J. LEVEQUE AND L. N. TREFETHEN, *Fourier analysis of the sor iteration*, IMA journal of numerical analysis, 8 (1988), pp. 273–279.
- [20] R. LI AND Y. YANG, *On well-posed boundary conditions for the linear non-homogeneous moment equations in half-space*, J. Stat. Phys., 190 (2023), p. 185.
- [21] W. LIU, Z. LIU, Z. ZHANG, C. TEO, AND C. SHU, *Grad’s distribution function for 13 moments-based moment gas kinetic solver for steady and unsteady rarefied flows: Discrete and explicit forms*, Comput. Math. Appl., 137 (2023), pp. 112–125.
- [22] I. MÜLLER AND T. RUGGERI, *Extended Thermodynamics*, vol. 37 of Springer tracts in natural philosophy, Springer-Verlag, New York, 1993.
- [23] A. RANA, M. TORRILHON, AND H. STRUCHTRUP, *A robust numerical method for the R13 equations of rarefied gas dynamics: Application to lid driven cavity*, J. Comput. Phys., 236 (2013), pp. 169–186.
- [24] N. SARNA, J. GIESSELMANN, AND M. TORRILHON, *Convergence analysis of Grad’s Hermite expansion for linear kinetic equations*, SIAM J. Numer. Anal., 58 (2020), pp. 1164–1194.
- [25] N. SARNA AND M. TORRILHON, *Entropy stable Hermite approximation of the linearised Boltzmann equation for inflow and outflow boundaries*, J. Comput. Phys., 369 (2018), pp. 16–44.
- [26] N. SARNA AND M. TORRILHON, *On stable wall boundary conditions for the Hermite discretization of the linearised Boltzmann equation*, J. Stat. Phys., 170 (2018), pp. 101–126.
- [27] O. SCHENK AND K. GÄRTNER, *Solving unsymmetric sparse systems of linear equations with PARDISO*, Future Generation Computer Systems, 20 (2004), pp. 475–487.
- [28] H. STRUCHTRUP, *Heat transfer in the transition regime: Solution of boundary value problems for Grad’s moment equations via kinetic schemes*, Phys. Rev. E, 65 (2002), p. 041204.
- [29] H. STRUCHTRUP, *Stable transport equations for rarefied gases at high orders in the Knudsen number*, Phys. Fluids, 16 (2004), pp. 3921–3934.
- [30] H. STRUCHTRUP AND M. TORRILHON, *Regularization of Grad’s 13 moment equations: Derivation and linear analysis*, Physics of Fluids, 15 (2003), pp. 2668–2680.
- [31] H. STRUCHTRUP AND M. TORRILHON, *Regularized 13 moment equations for hard sphere molecules: Linear bulk equations*, Phys. Fluids, 25 (2013), p. 052001.
- [32] W. SU, L. ZHU, P. WANG, Y. ZHANG, AND L. WU, *Can we find steady-state solutions to multiscale rarefied gas flows within dozens of iterations?*, Journal of Computational Physics, 407 (2020), p. 109245.
- [33] W. SU, L. ZHU, AND L. WU, *Fast convergence and asymptotic preserving of the general synthetic iterative scheme*, SIAM Journal on Scientific Computing, 42 (2020), pp. B1517–B1540.
- [34] L. THEISEN AND M. TORRILHON, *FenicsR13: A tensorial mixed finite element solver for the linear R13 equations using the FEniCS computing platform*, ACM Trans. Math. Softw., 47 (2021).
- [35] M. TORRILHON, *Two dimensional bulk microflow simulations based on regularized Grad’s 13-moment equations*, SIAM Multiscale. Model. Simul., 5 (2006), pp. 695–728.
- [36] M. TORRILHON AND N. SARNA, *Hierarchical Boltzmann simulations and model error estimation*, J. Comput. Phys., 342 (2017), pp. 66–84.
- [37] J. ZENG, R. YUAN, Y. ZHANG, Q. LI, AND L. WU, *General synthetic iterative scheme for polyatomic rarefied gas flows*, Computers & Fluids, 265 (2023), p. 105998.
- [38] L. ZHU, X. PI, W. SU, Z.-H. LI, Y. ZHANG, AND L. WU, *General synthetic iterative scheme for nonlinear gas kinetic simulation of multi-scale rarefied gas flows*, Journal of Computational Physics, 430 (2021), p. 110091.